THESIS FOR THE DEGREE OF DOCTOR OF PHILOSOPHY

Chemical-Looping Combustion and Chemical-Looping with Oxygen Uncoupling
- Use of Combined Manganese and Iron Oxides for Oxygen Transfer

Golnar Azimi

Division of Environmental Inorganic Chemistry
Department of Chemical and Biological Engineering
Chalmers University of Technology
Göteborg, Sweden, 2014

Chemical-Looping Combustion and Chemical-Looping with Oxygen Uncoupling
- Use of Combined Manganese and Iron Oxides for Oxygen Transfer
GOLNAR AZIMI
ISBAN 978-91-7597-083-7

© Golnar Azimi, 2014

Doktorsavhandlingar vid Chalmers tekniska högskola
Ny serie nr 3764
ISSN 0346-718X

Department of Chemical and Biological Engineering
Chalmers University of Technology
SE-412 96 Gothenburg
Sweden
Telephone + 46 (0)31-772 1000

Printed at Chalmers Reproservice AB
Göteborg, Sweden 2014

Abstract

Chemical-Looping Combustion (CLC) is an innovative technology that can be used for CO_2 capture. The CLC system is composed of two interconnected fluidized bed reactors. In the fuel reactor the added fuel reacts with an oxygen carrier, usually a metal oxide, to produce CO_2 and H_2O. The reduced metal oxide is then transported to the air reactor, where it is oxidized back to its original form, and the exit stream from this reactor will contain nitrogen and some unused oxygen. Chemical-Looping with Oxygen Uncoupling (CLOU) is very similar to CLC, but uses oxygen carriers with the ability to release gas phase oxygen, which reacts directly with the fuel, hence avoiding the necessity for a direct reaction between fuel and oxygen carrier. This could be especially advantageous for solid fuels, where gasification of char particles is otherwise a necessary step in the fuel conversion.

The objective of this work is to investigate two aspects of chemical-looping combustion. 1) hydrogen inhibition in steam gasification in CLC of solid fuels and 2) Chemical-Looping with Oxygen Uncoupling (CLOU) using combined Mn-Fe oxides.

The influence of the steam and hydrogen concentration on the rate of char conversion in CLC was investigated. The oxygen exchange model was found to be the best in describing hydrogen inhibition mechanism in steam gasification. Thus, a strong dependency between fuel gasification rate and hydrogen concentration was found, indicating that it is desirable to use a reactive oxygen carrier which removes hydrogen efficiently.

The thesis presents the first systematic study of oxygen carriers of iron-manganese oxides. Different combinations of iron and manganese oxide, with the Mn:Fe molar ratios varying between 4:1 and 1:4, were studied in a fluidized batch reactor to investigate release and uptake of oxygen and also their reactivity with respect to solid fuels, methane and synthesis gas (50/50% CO/H_2). Although these materials were shown to work excellently in the laboratory reactors, the mechanical strength needed improvement in order to have sufficient durability for commercial application. Consequently, work was undertaken to investigate the reactivity and attrition resistance of a series of supported Mn-Fe oxygen carriers with the aim of optimizing performance of this system. The support materials used were $MgAl_2O_4$, CeO_2, ZrO_2, Y_2O_3-ZrO_2 and Al_2O_3.

For the unsupported materials, reactivity was a clear function of the Mn/Fe ratio and temperature. At the higher reaction temperature, 950˚C, the oxygen carriers with a Mn/(Mn+Fe) molar ratio in the range of 25-33 %, show both the highest gas conversion of methane as well as the highest concentration of released oxygen. At 850˚C, on the other hand, the best methane conversion and oxygen release was seen for particles with a high Mn/(Mn+Fe) molar ratio of 67-80%.

Addition of support to materials with high Mn-content had the drawback that they were difficult to oxidize at 850˚C. Based on the results from the reactivity tests and the measured attrition rates, ZrO_2 support seems to be the most promising candidate among different supports for materials with high Mn-content.

Among the tested oxygen carriers, materials with a Mn:Fe molar ratio of 33:67 supported with Al_2O_3 showed the best behaviour, with a combination of high reactivity with fuel and low attrition. Also their oxidation with 5 vol% of oxygen was possible at temperatures higher than 850˚C. Low attrition, good reactivity and CLOU properties in combination with potentially low raw materials costs, make these materials highly interesting for the CLC application.

Keywords: CO_2 capture, Chemical-looping combustion, Chemical-looping with oxygen uncoupling, Iron-manganese oxide, ZrO_2, Al_2O_3

Acknowledgement:

Here, I would like to express my appreciation to all people who have supported and helped me during this work.

First and foremost, my deepest gratitude goes to my supervisor, Professor Anders Lyngfelt. Dear Anders, thanks a lot for all your patient guidance, enthusiastic encouragements and useful critiques during these years.

My heartfelt appreciations belong to my co-supervisor, Associate Professor Henrik Leion, who has been truly supportive every single day of this work. I owe you a lot Henrik. Thanks for everything.

A special gratefulness goes to my co-supervisor, Professor Tobias Mattisson, for his valuable advices and constructive comments during this project.

I would like to express my gratitude to Professor Jan-Erik Svensson as my examiner. Thanks for providing me with the opportunity to perform my research at Environmental Inorganic Chemistry.

I would like to extend my thanks to Associate Professor Magnus Rydén, for great collaborations and productive discussions.

I would also like to thank all the chemical-loopers: Pavleta Knutsson, Dazheng Jing, Martin Keller, Dongmei Zhao, Volkmar Frick, Sebastian Sundqvist, Carl Linderholm, Patrick Moldenhauer, Peter Hallberg, Jesper Aronsson, Matthias Schmitz, Malin Källén and Ulf Stenman.

Thanks and appreciation to the helpful colleagues at the Division of Environmental Inorganic Chemistry for creating a friendly working environment. My special thanks go to Charlotte Bouveng, Esa väänänen, Erik Brunius, Sandra Gustafson and Christina Anderson.

I would also express my thanks to the financer of this work, the Swedish Energy Agency, project number 32368-1.

I extend my heartfelt thanks to my family and friends for all their moral support and encouragement throughout my studies. I'm very grateful for the true love you give me.

Finally, my deepest gratefulness goes to my husband, Amin. I'm extremely thankful for having you in my life. Thanks for your care and being patient during my intensive works. Without your moral supports and encouragement, I couldn't do this work.

Golnar Azimi
Göteborg 2014

List of Publications

The thesis is based on the work contained in the following papers. In the text, they are referred by Roman numbers.

Paper I
Azimi, G.; Keller, M.; Mehdipoor, A.; Leion, H., Experimental evaluation and modeling of steam gasification and hydrogen inhibition in Chemical-Looping Combustion with solid fuel. *International Journal of Greenhouse Gas Control* **2012,** 11, (0), 1-10.

Paper II
Azimi, G.; Leion, H.; Rydén, M.; Mattisson, T.; Lyngfelt, A., Investigation of different Mn-Fe oxides as oxygen carrier for Chemical-Looping with Oxygen Uncoupling (CLOU). *Energy Fuels* **2013**, 27, (1), 367-377

Paper III
Azimi, G.; Leion, H.; Mattisson, T.; Lyngfelt, A., Chemical-looping with oxygen uncoupling using combined Mn-Fe oxides, testing in batch fluidized bed. *Energy Procedia* **2011,** 4, 370-377.

Paper IV
Azimi, G.; Rydén, M.; Leion, H.; Mattisson, T.; Lyngfelt, A., $(Mn_zFe_{1-z)y}O_x$ combined oxides as oxygen carrier for chemical-looping with oxygen uncoupling. *AIChE Journal* **2013,** 59, (2), 582-588

Paper V
Azimi, G.; Leion, H.; Rydén, M.; Mattisson, T.; Lyngfelt, A., Solid fuel conversion of iron manganese oxide as oxygen carrier for chemical-looping with oxygen uncoupling (CLOU). In *2nd International Conference on Chemical Looping*, Darmstadt, 26-28 September 2012.

Paper VI
Azimi, G.; Leion, H.; Mattisson, T.; Rydén, M.; Snijkers, F.; Lyngfelt, A., Mn-Fe oxides with support of $MgAl_2O_4$, CeO_2, ZrO_2 and Y_2O_3-ZrO_2 for Chemical-Looping Combustion and Chemical-Looping with Oxygen Uncoupling. *Industrial & Engineering Chemistry Research* **2014**, 53, (25), 10358-10365

Paper VII
Azimi, G.; Mattisson, T.; Leion, H.; Rydén, M.; Lyngfelt, A., Comprehensive study of Mn-Fe-Al oxygen-carriers for Chemical-Looping with Oxygen Uncoupling (CLOU). *Submitted for publication.*

Contribution report

Principal author, responsible for the experimental works and data evaluation in papers II-VII.
Principal author, responsible for part of the experimental works and data evaluation in paper I.

Related papers not included in the thesis

- Azimi, G.; Jing, D.; Leion, H.; Mattisson, T.; Rydén, M.; Lyngfelt, A., Iron-manganese oxide supported on $MgAl_2O_4$ and ZrO_2 as oxygen carrier for Chemical-Looping with Oxygen Uncoupling. In: *The 38th International Technical Conference on Clean Coal and fuel Systems*, Clearwater Florida, USA, 2nd-6th June **2013**

- Pour, N.M.; Azimi, G.; Leion, H.; Rydén, M.; Mattisson, T; Lyngfelt, A., Investigation of manganese-iron oxide materials based on manganese ores as oxygen carrier in chemical-looping with oxygen uncoupling (CLOU), *Energy Technology* **2014**, 2, (5), 469-479

- Pour, N.M.; Azimi, G.; Leion, H.; Rydén, M.; Lyngfelt, A., Production and examination of oxygen-carrier materials based on manganese ores and $Ca(OH)_2$ in chemical looping with oxygen uncoupling. *AIChE Journal* **2014**, 60, (2), 645-656

- Frohn, P.; Arjmand, M.; Azimi, G.; Leion, H.; Mattisson, T.; Lyngfelt, A., On the high-gasification rate of Brazilian manganese ore in chemical-looping combustion (CLC) for solid fuels. *AIChE Journal* **2013**, 59, (11), 4346-4354

- Mattisson, T., Jing D., Azimi, G., Rydén, M., van Noyen, J., and Lyngfelt, A., Using (MnxFe1-x)2SiO5 as oxygen carriers for chemical-looping with oxygen uncoupling (CLOU), paper presented at *AIChE Annual Meeting* November 3-8, San Fransisco **2013**

Table of Contents

Abstract III
Acknowledgement: IV
List of Publications V
Contribution report V
Related papers not included in the thesis VI
1. Introduction 1
1.1 The Greenhouse Effect and Global Warming 1
1.2 Carbon Capture and Storage (CCS) 1
1.3 Chemical-Looping Combustion (CLC) and Chemical-Looping with Oxygen Uncoupling (CLOU) 2
1.3.1 Chemical-Looping Combustion 2
1.3.2 Chemical-Looping with solid fuels 4
1.3.3 Oxygen Carriers 7
1.3.4 Combined Mn-Fe Oxide System 8
1.4 Objective 11
2 Experimental 12
2.1 Materials 12
2.2 Experimental Setup 12
2.3 Experimental Procedure and layout of the thesis 13
2.4 Data Evaluation 16
2.5 Characterization of Oxygen Carriers 19
3 Results 21
3.1 Steam gasification (paper I) 21
3.2 Oxygen carriers based on combined oxides of Mn-Fe (papers II-VII) 21
3.2.1 Oxygen Release of the Oxygen Carriers 21
3.2.2 Conversion of the Oxygen Carriers with Gaseous Fuel 28
3.2.3 Oxygen carrier reactivity with solid fuels 35
3.2.4 Oxidation of the oxygen carrier particles 42
3.2.5 Analysis of the Oxygen Carrier Particles 44
4 Discussion 49
5 Conclusions 52
6 References 54

1. Introduction

1.1 The Greenhouse Effect and Global Warming

The last three decades has been consecutively warmer at the surface of the earth than any previous decade since 1850[1]. The period between 1983-2012 was likely the warmest 30-year period of the last 1400 years in the northern hemisphere[1]. Since the 1950s, the ocean and atmosphere have warmed, sea level has risen, glaciers have decreased and the greenhouse gas concentrations have increased[1]. The Intergovernmental Panel on Climate Change (IPCC) announced in its third assessment report that the most important factor for global warming over the last 50 years is the increased concentrations of greenhouse gases in atmosphere[2], and carbon dioxide is considered as the most important anthropogenic greenhouse gas. Anthropogenic carbon dioxide emissions originate from sources like combustion for power generation, industrial processes and transportation. The carbon dioxide emitted from natural sources is 20 times larger than the emissions from human activities. But these natural sources are balanced by natural sinks like photosynthesis of plants and marine plankton[3].

Fossil fuel is the primary energy source globally, and thus the major source of anthropogenic emissions of carbon dioxide[4]. With a significant increase in the global energy demand, and the fact that fossil fuels are the primary source of energy, rigorous action for stabilizing the CO_2 level is needed[5]. Measures like improved energy efficiency and applying non-fossil energy alternatives such as nuclear, biomass, solar and wind energy will be important for reducing the CO_2 emissions. Given the strong dominance of fossil fuels, the increasing energy demand in developing economics and the need for fast and rapid reduction of emissions, it is likely that these technologies alone will not achieve the necessary reductions. An additional possibility to reduce the CO_2 emission is capturing CO_2 for storage in deep geological formations[3].

1.2 Carbon Capture and Storage (CCS)

For the concept of CCS, CO_2 is captured, compressed and stored in deep geological formations such as, depleted oil and gas reservoirs[6, 7], deep saline aquifers[8, 9] and coal bed formations[10]. The three main technologies being developed for CO_2 capture are: (1) Oxy-fuel combustion, which means removing nitrogen from air before combustion, (2) Post-combustion

capture, which means capturing CO_2 from flue gas in regular combustion and (3) Pre-combustion capture, which involves converting the fuel to hydrogen. In oxy-fuel combustion, pure oxygen in recycled flue gases is used instead of air for burning the fuel[11, 12]. In post-combustion capture the CO_2 is removed from the flue gases by passing it through process equipment that captures most of the CO_2. There are several technologies for post-combustion like absorption, adsorption, cryogenic separation and experimental technologies like membrane separation[5]. In pre-combustion the carbon content of the fuel will be removed before burning. The fossil fuel will be converted to hydrogen and carbon dioxide in a decarbonisation process[13] involving the following steps. In pre-combustion the fuel reacts with oxygen/air or steam in a gasifier and is partially oxidized to carbon monoxide and hydrogen. The gases produced from the gasification reactor react with steam in a catalytic shift reactor. The products from this step are hydrogen and carbon dioxide. These two gases are separated by a physical or chemical absorption process.

For the three technologies described above, costly and energy consuming gas separation equipment is inevitable. Another technology that can be used for CO_2 capture is Chemical-Looping Combustion (CLC). One of the most important benefits of this combustion technology is that CO_2 and H_2O are obtained separate from the other non-condensable flue gases, like excess O_2 and N_2, as a part of the process. By eliminating the need for separation of gases, costly and energy consuming equipment is avoided[14].

1.3 Chemical-Looping Combustion (CLC) and Chemical-Looping with Oxygen Uncoupling (CLOU)

1.3.1 Chemical-Looping Combustion

The CLC system is composed of two fluidized bed reactors (Figure 1). One of them is an air reactor where an oxygen carrier, usually a reduced metal oxide, denoted (Me_xO_{y-1}), is oxidized by air according to reaction 1. The oxygen carrier will then be transported to the second reactor, the fuel reactor. Here, the added fuel reacts with the oxygen carrier to produce CO_2 and H_2O, according to reaction 2. The reduced oxygen carrier is then again transported back to the air reactor to be re-oxidized back to its original state.

$$O_2(g) + 2Me_xO_{y-1} \leftrightarrow 2Me_xO_y \qquad (1)$$

$$C_nH_{2m} + (2n+m)Me_xO_y \leftrightarrow nCO_2 + mH_2O + (2n+m)Me_xO_{y-1} \qquad (2)$$

The total amount of heat released from the fuel reactor and the air reactor is equal to the heat released from ordinary combustion. Consequently, separation of CO_2 by CLC does not cause any direct losses in energy[14].

The flue gases from the fuel reactor consist ideally of only CO_2 and H_2O. The H_2O can be condensed and pure CO_2 can be compressed and transported to an appropriate storage location. The flue gases from the air reactor consist of nitrogen and a small amount of oxygen which can be released to the atmosphere. Since CO_2 is inherently separated from the nitrogen and oxygen in the flue gas, there is no direct energy penalty for the gas separation[14].

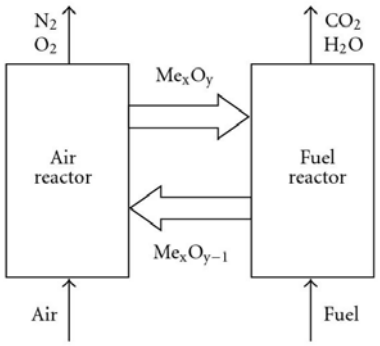

Figure 1- Schematic figure of the CLC process. Two interconnected fluidized bed reactors with circulating oxygen carrying particles are used in the combustion process

The basic idea of Chemical-Looping Combustion was first presented in a patent by Lewis and Gilliland in 1954 where it was proposed as a technology to produce pure carbon dioxide[15]. Later in 1994, Ishida and Jin proposed CLC as a technology for CO_2 capture in power plant[16]. In 2001, Lyngfelt et al. proposed two interconnected fluidized beds as a reactor design for the Chemical-Looping Combustion process[14]. Substantial research has been performed on CLC in the last years. Progress within this area has been reviewed by e.g Lyngfelt[17-19], Fan et al.[20], Fang et al.[21], Hossain et al.[22] and Adanez et al.[23]. The earlier published work on CLC focused on gaseous fuel, e.g.[24-30]. Solid fuels, like coal, are more abundant and cheaper than gaseous fuel. Consequently, it would be beneficial if the CLC process could be adapted to solid fuels. This is today an ongoing development with studies in both laboratory batch reactor[31-35] and circulating systems[36-41]. In solid fuel applications it is common to use cheaper alternatives as oxygen carrier such as natural mineral, ores[42-44], industrial by-products and wastes. The CLC process has been demonstrated in different units[45] of sizes 0.3 kW to 1 MW using solid fuel[46-51], gaseous fuel[52-54] and liquid fuel[55].

1.3.2 Chemical-Looping with solid fuels

1.3.2.1 Solid fuel conversion with steam gasification

In solid fuel application of CLC, metal oxide carriers and the char remaining after the volatiles release, do not react directly, but only via gaseous intermediates[56]. Therefore, fluidizing the mixture of fuel and particles in the fuel reactor with H_2O and/or CO_2 is proposed. The char will then be gasified by H_2O or CO_2 to H_2 and CO according to reactions 3 and 4. Subsequently, H_2 and CO can react with the oxygen carrier to produce CO_2 and H_2O[42].

$$C + H_2O \leftrightarrow CO + H_2 \qquad (3)$$

$$C + CO_2 \leftrightarrow 2CO \qquad (4)$$

At the temperatures of interest, the reactions of CO and H_2 with the oxygen carriers are rapid. On the other hand, the gasification reactions at these temperatures are comparably slow and therefore limit the conversion of the char[31, 32, 57]. The gasification of char is inhibited by CO and H_2[58-60]. Therefore, gasification in an inert sand bed is slower than in the presence of an oxygen carrier since the oxygen carrier effectively removes the inhibiting CO and H_2. Gasification with steam is generally faster than CO_2 gasification[61]. Keller et al. and Everson et al. did not observe inhibiting influence of CO on the steam gasification kinetics[62, 63]. Therefore, the CO inhibition on steam gasification is neglected in this work.

The steam gasification of char can be explained by the following two steps:

$$C_f + H_2O \xrightarrow{k_1} C(O) + H_2 \qquad (5)$$

$$C(O) \xrightarrow{k_2} CO + C_f \qquad (6)$$

By reaction (5), a $C(O)$ surface complex is formed and by reaction (6) this is converted to gaseous CO. In these reactions C_f is a free, active gasification site of carbon[58, 60].

There are three suggested mechanisms for explaining the hydrogen inhibition of steam gasification of carbon[58]. One is the oxygen exchange model in which it is assumed that reaction (5) is reversible[58, 60] according to:

$$C(O) + H_2 \xrightarrow{k_{-1}} C_f + H_2O \quad (7)$$

There are two hydrogen inhibition models in which reaction (5) is assumed irreversible. The first one is associative hydrogen adsorption in which a $C(H)_2$– complex[58, 60] is formed according to:

$$C_f + H_2 \underset{k_{-3}}{\overset{k_3}{\rightleftharpoons}} C(H)_2 \quad (8)$$

The other is dissociative hydrogen adsorption which assumes dissociative chemisorption of hydrogen[58, 60] according to:

$$C_f + \frac{1}{2}H_2 \underset{k_{-4}}{\overset{k_4}{\rightleftharpoons}} C(H) \quad (9)$$

The reaction rate can be explained by a Langmuir-Hinshelwood/Hougen-Watson (LHHW) type rate expression and is a function of p_{H_2O}, p_{H_2} and temperature[59]. The surface rate of reactions for these models can be expressed by the following equation[58].

Oxygen exchange model $$r_s = \frac{c_f k_1 p_{H_2O}}{1+\frac{k_1}{k_2}p_{H_2O}+\frac{k_1}{k_{-2}}p_{H_2O}} \quad (10)$$

Associative hydrogen adsorption model $$r_s = \frac{c_f k_1 p_{H_2O}}{1+\frac{k_1}{k_2}p_{H_2O}+\frac{k_3}{k_{-3}}p_{H_2}} \quad (11)$$

Dissociative hydrogen adsorption model $$r_s = \frac{c_f k_1 p_{H_2O}}{1+\frac{k_1}{k_2}p_{H_2O}+\frac{k_4}{k_{-4}}p_{H_2}{}^{0.5}} \quad (12)$$

In the above equation, c_f denotes the total concentration of active sites (C_f), k_i denotes the rate constants which depend on temperature and p_i denotes partial pressures. Hydrogen inhibition is accounted for by the term p_{H_2} in the denominator[60].

The mathematical expression of the rate equation for oxygen exchange model and associative hydrogen adsorption model is the same even if the rate constant expression is different [58].

1.3.2.2 Chemical-Looping with Oxygen Uncoupling

One option for using solid fuel is Chemical-Looping with Oxygen Uncoupling (CLOU) which is a variant of Chemical-Looping Combustion[64]. Here an oxygen carrier material which releases gas phase O_2 directly into the fuel reactor is used. In this method the solid fuel is converted through two steps. Firstly, oxygen is released by the oxygen carrier through reaction 13.

$$Me_xO_y \leftrightarrow Me_xO_{y-2} + O_2\,(g) \qquad (13)$$

Secondly, the fuel reacts with gas-phase oxygen, like in normal combustion, and produces CO_2 and H_2O according to reaction 14.

$$C_nH_{2m} + (n + m/2)\,O_2\,(g) \leftrightarrow nCO_2 + mH_2O \qquad (14)$$

The oxygen carrier is then transported to the air reactor and oxidized with air just as in CLC.

$$O_2 + Me_xO_{y-2} \leftrightarrow Me_xO_y \qquad (15)$$

The overall reaction in CLOU is identical to CLC, i.e. oxidation of hydrocarbon fuel to CO_2 and H_2O, but the mechanism for fuel conversion is different. This is especially important for char conversion. Since the char can react directly with O_2 released in CLOU, it does not need to be gasified, according to the reactions described above. Therefore, the main benefit with CLOU, as compared to CLC, is that the slow gasification of the solid fuel in CLC is eliminated[64]. The release of O_2 can also be beneficial for gaseous fuels since the O_2 released also can react with the fuel in the gas phase, thus reducing the need for good contact between gas and solids.

Previous works[34, 65] showed that the oxidation of solid fuels such as petroleum coke can be e.g. 45 times faster with CLOU, compared to ordinary CLC.

1.3.3 Oxygen Carriers

The selection of oxygen carrier is one of the key aspects of the CLC design. The metal oxide, which is used as an oxygen carrier, should have special features for CLC implementation. The main features can be stated as follows: sufficient reduction and oxidation rate, high fuel conversion to CO_2 and H_2O, low cost, low risks for health and environment, low tendency for agglomeration and low fragmentation and attrition[66, 67].

Oxide systems of transition metals are possible candidates for oxygen carrier materials, such as Mn_3O_4/MnO, Fe_2O_3/Fe_3O_4, NiO/Ni and CuO/Cu[22-24, 66-71]. Support materials can be combined with the metal oxide to provide a higher reaction surface area and also to increase the mechanical strength of the metal oxide for preventing attrition. Al_2O_3, ZrO_2, TiO_2 or SiO_2 are examples of materials that have been applied as support material[67].

In addition to the properties for a CLC oxygen carrier, a feasible CLOU oxygen-carrier should be possible to oxidize in the air reactor and also release gaseous O_2 in the fuel reactor at appropriate temperature and oxygen partial pressures[64], provide sufficiently fast reaction kinetics for the O_2 uncoupling and the oxidation reactions, and have a decently high content of active oxygen. Many commonly proposed oxygen carriers for Chemical-Looping Combustion such as NiO and Fe_2O_3 fail to satisfy the CLOU requirements, i.e. they cannot release gas phase O_2 at relevant conditions.

Some metal oxides of manganese, copper, cobalt have an appropriate equilibrium pressure of gaseous oxygen within the range of 700 to 1200˚C. However, Co_3O_4/CoO is unsuitable due to high cost and toxicity. CuO/Cu_2O appears promising[34, 65] but the fairly high cost and the low melting point of metallic Cu, 1085˚C, are disadvantages. Although metallic Cu will not be formed during ideal CLOU conditions, it is likely that there will be some formation of Cu in the fuel reactor due to direct reaction with reactive gases such as volatile matter. Applying pure manganese oxide in CLOU is troublesome because the relevant equilibrium concentrations applicable for CLOU with Mn mean operation at relatively low temperatures, and it has been found that the oxidation of Mn_3O_4 to Mn_2O_3 is slow at relevant temperatures[72]. However, this temperature limitation can be overcome by combining manganese oxide with other materials. Iron, nickel, silicon, magnesium and calcium are examples of materials that can be combined with manganese oxides to change its characteristics[73-77]. The Fe-Mn system appears to be

especially promising due to favourable thermodynamics[78, 79] which is also confirmed by the experimental work in this thesis.

1.3.4 Combined Mn-Fe Oxide System

A thermal analysis of the Mn_2O_3/Mn_3O_4 oxides system has been performed by Mattisson et al.[64]. This material releases oxygen in the gas phase through the following reversible reaction:

$$6Mn_2O_3 \leftrightarrow 4Mn_3O_4 + O_2\,(g) \qquad \Delta H_{850}=193.9 \ \text{kJ/mol}\ O_2 \qquad (16)$$

For Mn_2O_3/Mn_3O_4 the equilibrium pressure of O_2 is equal to that of O_2 in air at 899°C. This means that Mn_2O_3 releases oxygen in air at temperature above 899°C and Mn_3O_4 takes up oxygen at temperatures below this temperature[64]. The oxidized particles, i.e. Mn_2O_3, are transported to the fuel reactor in which the partial pressure of O_2 is low, thus they will decompose and release gaseous O_2. The amount of oxygen released and the maximum concentration of oxygen are dependent on the fuel reactor temperature. The fuel reactor temperature is influenced by the temperature of the incoming particles, the circulation rate and heat of reaction in the fuel reactor. For Mn_2O_3/Mn_3O_4 the overall reaction in the fuel reactor is exothermic, which results in a temperature increase in the fuel reactor and consequently the oxygen carrier would be able to release higher concentration of gaseous oxygen. A higher partial pressure of oxygen will improve the overall conversion rate for solid fuels[64].

The relevant equilibrium concentrations applicable for CLOU with Mn would mean operation at relatively low temperatures. Thus, oxidizing Mn_3O_4 to Mn_2O_3 in the air reactor with an oxygen concentration of maximum 5% is only possible at temperatures below 800°C[64]. Higher oxygen concentration should be avoided in order to have a combustion process at a reasonable air ratio. Experiments with Mn_3O_4 suggest that this temperature is too low to have a sufficiently high reactivity[72]. Several recent studies have shown that it is possible to alter the thermodynamic properties of manganese oxides by combining them with other cations like iron, nickel, silicon, magnesium and calcium. Many such combined oxides have faster kinetics for O_2 release, and are also capable to operate at higher temperatures than the unmodified Mn_2O_3-Mn_3O_4 system. Notably, many variants of the perovskite structure $CaMnO_{3-\delta}$ have been shown to have excellent properties for chemical-looping applications[75, 77, 80]. In the perovskite structure, the oxygen non-stoichiometry, δ, changes depending on the partial pressure of oxygen and temperature[81]. At constant temperature, by decreasing surrounding oxygen partial pressure, the oxygen deficiency

in perovskite increases by releasing gaseous oxygen to the surrounding. The combined manganese oxides have been examined as oxygen carrier in CLC and CLOU. Shulman et al.[73, 74] tested several combinations for example Mn/Mg, Mn/Ni, Mn/Si as well as the Fe/Mn oxide system.

Due to the low price and favourable environmental properties of manganese and iron oxides, the Fe/Mn system is of interest for the development of CLOU. There are also a number of ores and minerals with a suitable Fe/Mn fraction that potentially could be used as oxygen carriers. Work that has focused only on the Fe/Mn system has been performed by Ksepko et al.[82], Lambert et al.[83], Fossdal et al.[84] and Rydén et al.[85]. However, only in the work of Ryden et al. was the CLOU effect of this system investigated.

In this work a binary phase diagram of the $(Mn_zFe_{1-z})_yO_x$ system has been calculated with the software FactSage using the FToxid database, and this is shown in Figure 2, cf. paper II. The diagram is calculated for an O_2 partial pressure of 0.05 atm, which may be an appropriate basis with respect to the exiting O_2 concentration of the air reactor in a CLOU process. The phase diagram of iron-manganese oxide has also been investigated experimentally by Kjellqvist et al.[86], Muan and Sōmiya[87], Wickham[79] and Crum et al.[78], although in air. Results obtained with FactSage for this system agrees well with literature data, e.g. Kjellqvist and Selleby[86]. Thus the phase diagram gives an accurate representation of the system behaviour, although available thermodynamic data for combined oxides of iron and manganese are not precise in detail[78].

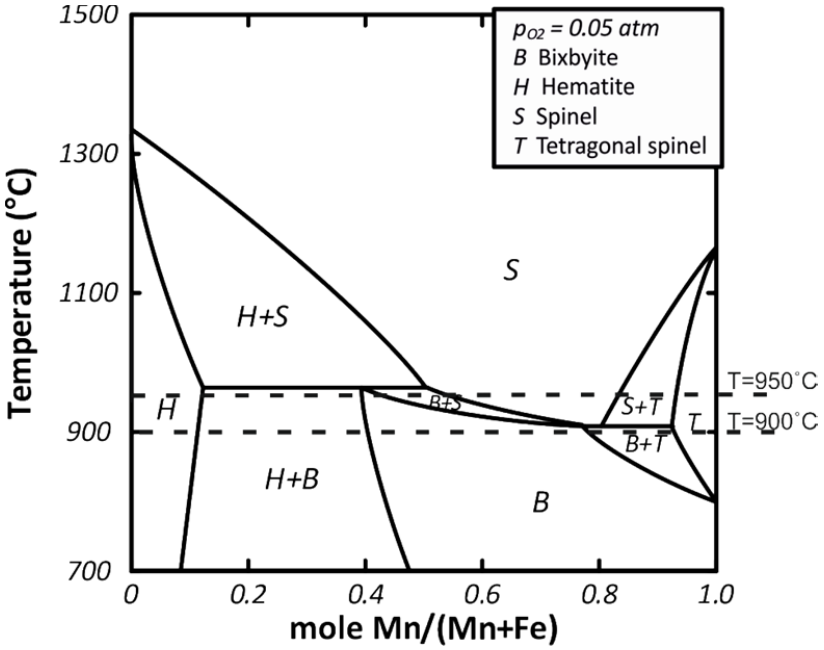

Figure 2- Phase diagram of $(Mn_yFe_{1-y})O_x$ in an atmosphere with an O_2 partial pressure of 0.05 atm calculated with the software FactSage

Figure 2 indicates that the stable phases at low temperature are the fully oxidized states i.e. hematite and bixbyite, both with the general formula $Fe_{2-x}Mn_xO_3$ or $(Fe,Mn)_2O_3$, whereas the reduced spinel phases $(Fe,Mn)_3O_4$ and the tetragonal spinel, hausmannite (Mn_3O_4), are stable at high temperature. There are also two-phase areas in which both forms i.e. bixbyite/hematite and spinel, coexist at intermediate temperatures. Moving from low to high temperatures will result in a phase change from $(Fe,Mn)_2O_3$ to $(Fe,Mn)_3O_4$ which is accompanied by oxygen release (reaction 17) equivalent to 3.3-3.4% change of mass.

$$6(Mn,Fe)_2O_3 \leftrightarrow 4(Mn,Fe)_3O_4 + O_2(g) \qquad (17)$$

A similar release of O_2 will occur when moving from a high to a low partial pressure of oxygen, which is what happens when an oxygen carrier is transported from the air to the fuel reactor of a CLOU system. Thus reaction 17, decomposition of bixbyite to spinel, should happen spontaneously in the fuel reactor. The oxygen released would then be instantly consumed by the fuel, facilitating further O_2 release. In the air reactor, reaction 17 is reversed, i.e. bixbyite is recreated by oxidation with air.

Figure 2 shows that the phase transition boundary between bixbyite and the two phase region of bixbyite and spinel occurs at higher temperature when the amount of Fe is increased. However, the phase transition between fully oxidized phase $(Mn,Fe)_2O_3$ and fully reduced phase needs to pass a two phase area where both phases coexist. This means that, for a constant oxygen partial pressure, a certain temperature change is needed to accomplish a complete phase change between the fully oxidized and fully reduced phases. The same will also apply to the needed change in oxygen concentration, if a change in oxygen concentration is used to achieve this phase change. The height of the two-phase area in Figure 2 should correspond to the change in temperature or O_2 partial pressure that will be required to force reaction 17 into completion. Figure 2 also indicates that the smallest temperature change is needed where the manganese fraction is 60-80 mole% since the height of two-phase region of bixbyite and spinel is low there.

1.4 Objective

This thesis concerns investigation of various aspects of chemical-looping with both gaseous and solid fuels. The main focus is the investigation around a new set of oxygen carriers based on the combined oxides of Fe and Mn. These materials have interesting oxygen uncoupling properties, and this is the first systematic investigation of this type of materials as oxygen carriers for chemical-looping combustion. The uncoupling properties make them especially interesting for solid fuels, but they also have advantages with respect to gaseous fuels. Hence, a systematic investigation of a number of pure Fe-Mn-O materials with varying ratios of Fe/Mn was conducted, see papers II-V. These investigations clearly demonstrate the feasibility of using such oxygen carriers, with remarkable oxygen release rates for certain materials. Still, the mechanical strength and attrition resistance were not sufficient for use in a real CLC system. Thus oxygen carrier particles of the same active systems were produced with a variety of support materials, including ZrO_2 and Al_2O_3, see papers VI and VII.

Furthermore, the potential effect of oxygen carriers on hydrogen inhibition of steam gasification was investigated in paper I, in a study where both hydrogen and steam concentration were varied.

2 Experimental

2.1 Materials

The oxygen carriers studied in this work are particles with different molar ratios of Fe/Mn, varying between 4:1 and 1:4, and also supported Mn-Fe materials with addition of $MgAl_2O_4$, CeO_2, ZrO_2, Y_2O_3-ZrO_2 and Al_2O_3. All the materials were produced by spray-drying at VITO in Belgium. After spray-drying, the fraction in the required particle size range was obtained by sieving. In order to obtain oxygen carrier particles with sufficient mechanical strength, calcination was performed in air at 1200˚C, 1100˚C or 950˚C, for 4 h. After calcination, the particles were sieved again to the size range 125-180 μm. Details about the production method can be found in the paper II.

An example of denotation for the samples without support in this work is M20F1100, where M denotes Mn_3O_4 and the digits after M represents the manganese oxide mass fraction of the sample. Further, F denotes iron oxide and the digit after F denotes the calcination temperature of the sample.

For supported materials, M denotes Mn_3O_4 and the digits after M represents the mass fraction of Mn_3O_4 in the sample. Further, F denotes Fe_2O_3, the material after F denotes the applied support, the following digits show the mass fraction of support in the sample and the last digits indicate the calcination temperature of the sample.

In the study of steam gasification, quartz sand, ilmenite, oxide scales and nickel oxide have been used as the bed materials. The oxide scales are a waste product from the steel industry. Details are given in paper I.

The solid fuels which were used in some of the experiments are petroleum coke, a Colombian coal and wood char, see paper I, III-V and VII for details.

2.2 Experimental Setup

The experiments were performed in a fluidized bed quartz reactor which has a length of 820 mm and a porous quartz plate of 22 mm in diameter placed 370 mm from the bottom. The laboratory setup incorporating this reactor is shown in Figure 3. This system is not a circulating fluidized bed system, but instead emulates circulation by exposing the oxygen carriers alternatingly to oxidation with air and a reduction in a fuel/steam mixture. The system is flushed between those cycles by an inert gas flow (nitrogen). All experiments were repeated at least two

times. To generate the required steam for the reduction period of the solid fuel experiments, a steam generator was used (Cellkraft Precision Evaporator E-1000). When using solid fuels, 300 ml/min of inert sweep gas was introduced to the system at the top of the reactor together with the solid fuel to ensure that the pulverized fuel does not get stuck in the feed and that there is a sufficient dry gas flow to the analyzer. However this sweep gas did not enter the hot reaction zone of the reactor. The gas from the reactor was led to an electric cooler for removing water and then to a Rosemount NGA 2000 Multi-Component gas analyzer, which measured the concentrations of CO, CO_2, CH_4, H_2 and O_2 in the flue gas as well as the volumetric flow rate. The temperature was measured 5 mm under and 10 mm above the porous quartz plate using Pentronic CrAl/NiAl thermocouples with inconel-600 enclosed in quartz shells. The temperature presented in the paper is the set-point temperature, i.e. the temperature at the beginning of the reduction when no chemical reaction occurs. From high frequency measurements of the pressure drop over the reactor, it was possible to see if the bed was fluidized.

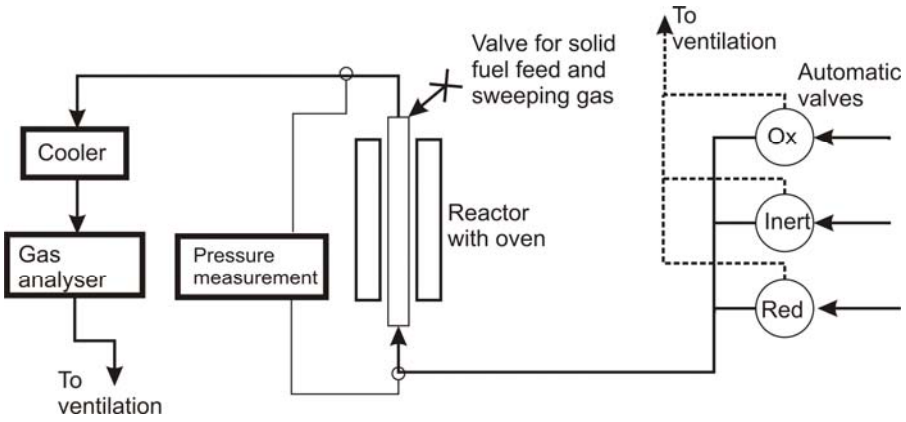

Figure 3- Schematic layout of the laboratory setup

2.3 Experimental Procedure and layout of the thesis

In paper II, the CLOU property of unsupported iron-manganese oxide is examined by decomposition in N_2 and moreover the reaction with both methane and synthesis gas (50/50% CO/H_2) was examined. Normally a sample of 15 g of oxygen carrier particles with diameter of 125-180 μm was placed on the porous plate and the reactor was then heated to the temperature of interest in a flow of 900 mL_n/min containing 5% O_2 in N_2. This was done in order to prevent uncontrolled release of oxygen and to ensure that the oxygen carriers are adequately oxidized

prior to the experiments. The use of 5% O_2 during oxidation corresponds to the exiting stream in an air reactor with an air ratio of approximately 1.2 in a real chemical-looping system. As the required conditions were reached, the particles were fluidized by 600 mL_n/min of pure N_2, and the outlet oxygen concentration was measured during the inert period. The particles were exposed to consecutive cycles of oxidizing and inert periods at a temperature of 900˚C. The particles were also exposed to periods in which the temperature for oxidation was still 900˚C but the temperature was raised to 1000˚C during the inert period, see Table 1. The periods in which the pure nitrogen is the only fluidizing gas in the reactor, are called non-fuel periods or inert periods. The non-fuel period helps to give better understanding of the O_2 uncoupling behaviour since N_2 is inert and does not interfere with the released oxygen. For reactivity evaluation, the particles were exposed to 365 mL_n/min CH_4 or 450 mL_n/min synthesis gas (syngas, 50/50% CO/H_2) at 950˚C. The oxidation and the reduction periods were separated by an inert period during which the reactor was purged from reactive gases and gaseous products by introduction of N_2.

Some of the particles were also examined at a temperature of 850˚C, both decomposition in nitrogen and reactivity test with methane. Table 1 presents a detailed plan of the experiments.

Table 1- Experimental plan for testing of the oxygen uncoupling behaviour and reactivity with gaseous fuel for unsupported Fe-Mn materials. F_x is flow in period x, i.e. Ox(idation), Red(uction) and In(ert)

No of cycles	**Reducing gas**	**F_{Ox} (mL_n/min)**	**F_{In} (mL_n/min)**	**t_{In} (s)**	**F_{Red} (mL_n/min)**	**t_{Red} (s)**	**T_{Ox} (˚C)**	**T_{Red} (˚C)**
3	nitrogen	900	600	360	-	-	900	900
1	nitrogen	900	600	360	-	-	900	900 → 1000
3	methane	900	600	60	365	20	950	950
3	syngas	900	600	60	450	80	950	950
3	nitrogen	900	600	360	-	-	900	900
3	nitrogen	900	600	360	-	-	900	900→1000
3	nitrogen	900	600	360	-	-	850	850
3	methane	900	600	60	365	20	850	850
3	nitrogen	900	600	360	-	-	850	850

The particles with a calcination temperature of 1100˚C were selected as a basis for all experiments and were examined at three different temperatures, 850˚C, 900˚C and 950˚C. For materials calcined at 950˚C, only temperatures which were judged to be interesting were examined. Thus, the samples with a Mn/(Mn+Fe) molar ratio lower than 50% were examined at 900˚C and 950˚C and the materials with a Mn/(Mn+Fe) molar ratio higher than 60%, were tested at 850˚C. This was motivated by the results with the materials calcined at 1100˚C and also by the thermodynamic analysis which clearly shows why lower temperature should be used for a high Mn-fraction and vice versa, cf. Figure 2.

Paper II is a basis for the other CLOU publications, and those unsupported Fe-Mn materials that showed the best behaviour with respect to oxygen release and reactivity with gas here, have been investigated with solid fuel in the papers III to V. The solid fuel experiments without steam are meant to obtain conclusive evidence that the main mechanism in the oxygen carrier's oxygen release and high reactivity is through oxygen uncoupling and not direct reaction of oxygen carrier and methane. This is due to the fact that in the experiments with solid fuel the possibility of direct solid-solid reaction in the fluidized bed is essentially eliminated.

In paper III, the reactivity of M33F1100 particles was investigated with two solid fuels: Colombian coal and petroleum coke.

In paper IV, the oxygen carrier particles M80F950 was alternatingly exposed to O_2/N_2 mixture, and reducing periods in which different amounts of wood char were introduced to the bed of oxygen carrier particles.

In Paper V, the author examined oxygen carrier materials with Mn:Fe molar ratios in the range 67:33 up to 80:20, in order to see how the iron content affects oxygen release and uptake with addition of devolatilized wood char in N_2.

Considering the fact that the Mn-Fe combined system showed very interesting properties with respect to reactivity, but because of problems with respect to mechanical stability, it was motivated to study the use of support materials for combined oxides of Fe-Mn. In paper VI, the CLOU property and the reaction with both methane and synthesis gas of the oxygen carriers particles with Mn:Fe molar ratio of 75:25 with addition of $MgAl_2O_4$, CeO_2, ZrO_2 and Y_2O_3-ZrO_2 as support were investigated.

Paper VII includes a comprehensive study of the use of Al_2O_3 as oxygen carrier. Al_2O_3 has been found to be a suitable support for iron oxide[88-91], and thus it was decided to also pursue this

system for the combined Mn-Fe system. The oxygen carriers studied in paper VII are particles with a Mn:Fe molar ratio of 80:20 and 33:67 with addition of different amounts of Al_2O_3 as support. For initial screening of these materials, the CLOU property and the reaction with both methane and synthesis gas of the oxygen carrier particles were examined. Four of the more interesting samples from the initial screening were selected for further testing with syngas and char at different temperatures.

The work done in paper I investigates and models the influence of the steam and hydrogen concentration in the fuel reactor on the rate of solid fuel conversion using oxygen carriers and sand. The oxygen carriers used were ilmenite, nickel oxide and oxide scales. Different fractions of steam and hydrogen were added to the fluidizing stream. Additionally, gasification experiments of fuel particles pretreated in mixtures of H_2 and N_2 were performed in order to determine the reversibility of the observed hydrogen inhibition.

Detailed information regarding experimental setup and procedure can be found in the respective papers.

2.4 Data Evaluation

The degree of oxygen carrier conversion, *X*, describes the extent to which the oxygen carriers are oxidized and is defined as follows:

$$X = \frac{m - m_{red}}{m_{ox} - m_{red}} \qquad (18)$$

Here m is the actual mass of the sample, m_{ox} is the mass of the fully oxidized sample i.e. bixbyite, and m_{red} is the mass of the sample in its fully reduced form i.e. spinel. The degree of conversion of oxygen carriers as a function of time during reduction with methane and syngas is calculated from the outlet gas concentrations using equation 19 and equation 20, respectively.

$$X_i = X_{i-1} - \int_{t_0}^{t_1} \frac{1}{n_0 P_{tot}} \dot{n}_{out} (4 p_{CO_2,out} + 3 p_{CO,out} + 2 p_{O_2,out} - p_{H_2,out}) dt \qquad (19)$$

$$X_i = X_{i-1} - \int_{t_0}^{t_1} \frac{1}{n_0 P_{tot}} \dot{n}_{out} (2 p_{CO_2,out} + p_{CO,out} + 2 p_{O_2,out} - p_{H_2,out}) dt \qquad (20)$$

Correspondingly, the degree of conversion is determined using the relationship 21 for the inert period and by equation 22 for the oxidizing period.

$$X_i = X_{i-1} - \int_{t_0}^{t_1} \frac{1}{2n_0 P_{tot}} (\dot{n}_{out} p_{O_2,out}) dt \qquad (21)$$

$$X_i = X_{i-1} + \int_{t_0}^{t_1} \frac{1}{2n_0 P_{tot}} \dot{n}_{out} ((p_{O_2,in}(P_{tot} - p_{O_2,out})/(P_{tot} - p_{O_2,in})) - p_{O_2,out} - p_{CO_2,out}) dt \qquad (22)$$

Moreover, the degree of conversion during reduction with solid fuel is described using equation 23.

$$X_i = X_{i-1} - \int_{t_0}^{t_1} \frac{1}{2n_0 P_{tot}} \dot{n}_{out} (p_{CO_2,out} + 0.5 p_{CO,out} + p_{O_2,out} - (O_2/C)_{fuel} p_{c,tot} + (0.5(H_2/C)_{fuel} p_{c,tot} - 0.5 p_{H_2,out} - p_{CH_4,out})) dt \qquad (23)$$

In the equations presented above, X_i is the conversion as a function of time for a period i, X_{i-1} is the degree of conversion after the foregoing period, t_0 and t_1 are the times for the start and the end of the period, n_0 is the moles of active oxygen in the fully oxidized sample, and $\dot{n}_{out}$ is the molar flows of dry gas entering the analyser. Normally, when using gaseous fuels, the periods are rather short but with a high degree of variability with respect to the gas conversion, resulting in rather large flow variations. Thus, in this work the flow measured in the gas analyzers was used when calculating the conversion. But for solid fuel experiments, the flow is calculated from incoming flows and concentrations. This choice is based on what is judged to give the most accurate results. P_{tot} is the total pressure, $p_{i,out}$ is the outlet partial pressures of gas component i after removal of water vapour. $p_{O2,in}$ is the inlet partial pressure of oxygen. $(O_2/C)_{fuel}$, $(H_2/C)_{fuel}$ are the estimated molar ratios of oxygen and hydrogen to carbon in the fuel; and $p_{c,tot}$ is the total partial pressure of carbon, i.e. $p_{CO2,out} + p_{CO,out} + p_{CH4,out}$. The hydrogen partial pressure $p_{H2,out}$ was not measured online during the gas fuel experiments, but it was calculated by the assumption of having equilibrium water gas shift reaction.

$$CO + H_2O \leftrightarrow CO_2 + H_2 \qquad (24)$$

The oxygen ratio of the oxygen carrier, R_0, is defined as below:

$$R_0 = \frac{m_{ox} - m_{red}}{m_{ox}} = \frac{m_0}{m_{ox}} \qquad (25)$$

In the equation above, m_0 is the mass of active oxygen in the unreacted oxygen carrier. The R_0 value for particles with different Mn:Fe molar ratios is in the range 0.0335-0.0337 when moving between $(Mn_zFe_{1-z})_2O_3$ and $(Mn_zFe_{1-z})_3O_4$. Hence, theoretically removing the excess of 3 wt% oxygen can occur through this reaction by CLOU.

In order to be able to compare oxygen carrier materials which contain different amounts of oxygen, a mass-based conversion, ω, is defined as follows:

$$\omega = \frac{m}{m_{ox}} = 1 + R_0(X - 1) \qquad (26)$$

For analysis of gas conversion, the fraction of CO_2 in the outlet gas flow was calculated on dry basis as follows:

$$\gamma = \frac{p_{CO_2}}{p_{CH4} + p_{CO_2} + p_{CO}} \qquad (27)$$

In paper I, the steam gasification of char was studied. Here, the degree of carbon conversion X_c is used to describe the progress of the gasification.

$$X_C = \frac{m_C(t)}{m_{total}} \qquad (28)$$

Here m_c (t) denotes the mass of carbon already gasified at time t and m_{total} denotes the total mass of carbon converted during one cycle. The mass of carbon is determined by integration of the concentrations of the carbon containing product gases during the reduction, assuming that the ideal gas law is valid.

$$m_C(t) = M_C \int_0^t \dot{n}_{out}(t)[p_{CO_2,out}(t) + p_{CO,out}(t) + p_{CH_4,out}(t)]dt \qquad (29)$$

Here M_c denotes the molar mass of carbon. The total mass of carbon is determined in a similar way, but here the concentration profiles are integrated from the beginning of the gasification until the end of the oxidation phase. Therefore, the amount of carbon that was not gasified during the reduction but burnt off with synthetic air during oxidation is also included in m_{total}.

$$m_{total} = M_C \int_0^{t_{total}} \dot{n}_{out}(t)[p_{CO_2,out}(t) + p_{CO,out}(t) + p_{CH_4,out}(t)]dt \qquad (30)$$

The rate of carbon conversion normalized with respect to the amount of carbon initially present in the reactor, r_W, is defined as:

$$r_W = \frac{dX_C}{dt} = \frac{\dot{m}_C}{m_{total}} \qquad (31)$$

The instantaneous rate of conversion normalized with respect to the amount of carbon present at time t, r, is defined as:

$$r = \frac{r_W}{1 - X_C} \qquad (32)$$

In this work r is used to express the rate of fuel conversion.

2.5 Characterization of Oxygen Carriers

The analysis of the phase compositions of the oxygen carrier particles was performed on a Siemens D5000 powder X-ray diffractometer (Cu Ka1, k = 1.54056 Å). The shape and morphology of fresh and tested oxygen carriers were observed using a FEI, Quanta 200 Environmental Scanning Electron Microscope FEG (SEM). The bulk density of all materials, sized 125-180 μm, was measured by weighing 5 ml of particles filled in a graduated cylinder. The BET surface area of the particles was measured by N_2-absorption using Micromeritics, ASAP 2020.

The crushing strength, i.e. the force needed to fracture the particles, was examined using a Shimpo FGN-5 crushing strength apparatus. For each sample 30 different particles of size 180–250 μm were tested and the mean value gives the crushing strength. Attrition resistance of the particles was investigated in a jet cup rig previously used for the study of attrition of oxygen carriers by Rydén et al.[92]. The apparatus consists of a 39 mm high conical cup with an inner diameter of 13 mm in the bottom, and 25 mm in the top. At the bottom of the cup, there is a nozzle with diameter of 1.5 mm which injects air with a velocity of approximately 100 m/s. The cup is located at the bottom of a 634 mm high cone with a maximum diameter of 216 mm. A particle filter with a 0.01 μm filter element is at the top of the apparatus. At the start of the experiments the filter was weighed. Approximately 5 g sample was placed in the cup. Every 10 minutes the filter was weighed and the test was performed for 1 h. It should be noted that the attrition index is the result of a particular testing procedure so it should not be interpreted as the expected lifetime of oxygen carrier particles in a real chemical looping combustor. The jet cup

tests at room temperature provide an indication concerning the feasibility of different oxygen carrier materials[92].

3 Results

3.1 Steam gasification (paper I)

Previously, Leion et al.[42, 93] showed that the fuel gasification is about two times faster in the presence of oxygen carrier than using sand. This can be explained by removal of H_2 which can inhibit the gasification. In paper I, the influence of the steam and hydrogen concentration in the fuel reactor on the rate of solid fuel conversion in chemical-looping combustion was investigated using oxygen carriers and sand. The oxygen carriers used were ilmenite, nickel oxide and oxide scales. Different fractions of steam and hydrogen were added to the fluidizing stream. Higher steam concentration increases the rate of char conversion and, higher hydrogen concentration decreases the rate as a result of hydrogen inhibition.

The oxygen exchange model was found to be the best in describing hydrogen inhibition mechanism in steam gasification for CLC experiments of wood char and Colombian coal. In equations 10-12, hydrogen inhibition is accounted for by the term p_{H_2} in the denominator. The hydrogen inhibition is more significant for the oxygen exchange model since p_{H_2} is in square root for the dissociative hydrogen adsorption model. Thus, a strong dependency between fuel gasification rate and hydrogen concentration was found. Consequently, to achieve high rates of char conversion in CLC with solid fuels, it is desirable to use an oxygen carrier which consumes and thereby removes hydrogen efficiently from the reaction zone.

3.2 Oxygen carriers based on combined oxides of Mn-Fe (papers II-VII)

A large number of oxygen carrier particles based on the system Mn-Fe have been manufactured by spray-drying and evaluated with respect to i) the oxygen uncoupling properties, ii) reactivity with methane and syngas, iii) reactivity with solid fuels and iv) physical characterisation including attrition resistance. The main aspects are summarized below, but for details, the reader is referred to the papers attached to the thesis.

3.2.1 Oxygen Release of the Oxygen Carriers

The oxygen release ability of the oxygen carrier particles was investigated by exposure to N_2 in the fluidized bed reactor, see Table 1. Figure 4a illustrates oxygen concentration as a function of oxygen carrier conversion, X, during the final periods with N_2. Unsupported materials with

different Mn/Fe ratios were used. The inert periods had a duration of 360 s and were made after the fuel cycles.

As can be seen in Figure 4a, the particles with a Mn/(Mn+Fe) molar ratio of 20-40% released oxygen during the entire non-fuel period. The outlet volume fraction of oxygen for these materials after 360 s is in the range of 0.2% to 0.4%. The other materials did not release any oxygen during the non-fuel periods. The latter can be explained by the phase diagram, Figure 2, which shows that the reduced oxygen carriers with a Mn/(Mn+Fe) molar ratio of more than 40% would be difficult to oxidize to bixbyite in 5% of oxygen at 900˚C since they are very close to the phase region of bixbyite + spinel or spinel. The most likely reason is that the reaction is kinetically hindered when conditions are close to those where the reduced phase is stable. Consequently, according to the results from the non-fuel periods, M25F950, M33F950 and M33F1100 show the best behaviour in term of release of oxygen at this temperature.

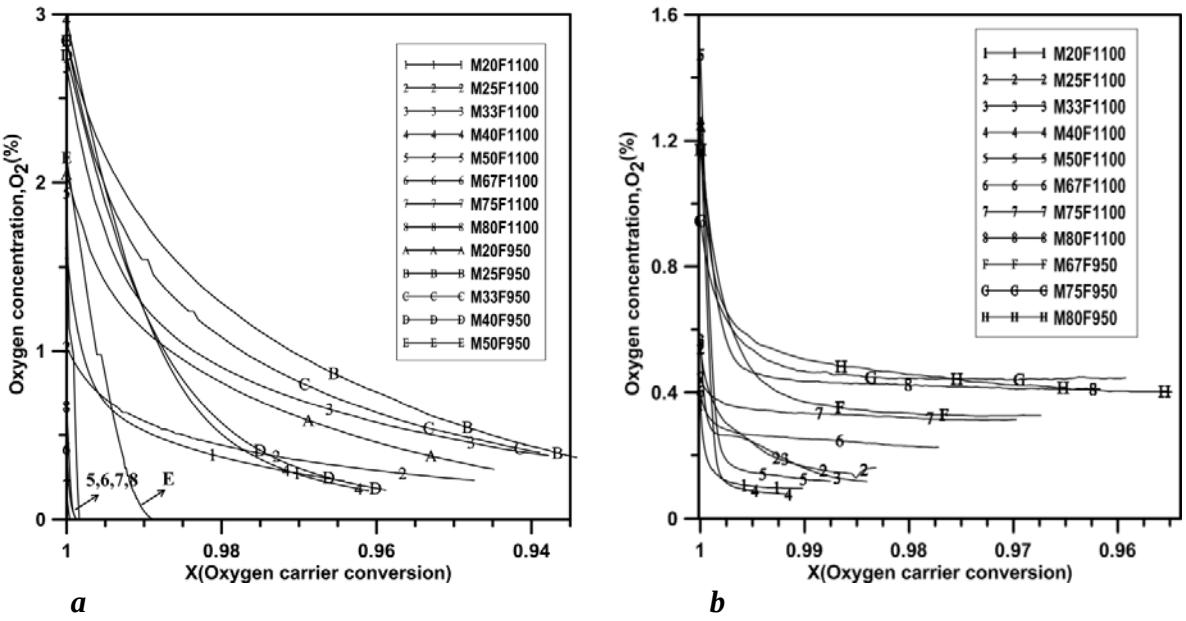

Figure 4-Oxygen concentration as a function of the oxygen carrier conversion, X, during the final non-fuel periods for 360 s (a) at 900˚C and (b) at 850˚C for unsupported Mn-Fe materials (paper II)

However, applying a temperature lower than 900˚C in the air reactor should make it possible to oxidize the oxygen carriers with a Mn/(Mn+Fe) molar ratio higher than 50% to bixbyite.

Hence, the materials were also tested at a lower temperature, i.e. 850˚C. Figure 4b shows the oxygen concentration as a function of oxygen carrier conversion during non-fuel periods for 360 s at 850˚C.

As seen in Figure 4b, the oxygen release from the oxygen carriers with a Mn/(Mn+Fe) ratio higher than 50 mole%, increases when reducing the temperature to 850˚C and decreases for material with a Mn/(Mn+Fe) ratio of less than 50 mole%. The particles with a calcination temperature of 950˚C show better oxygen release than the particles calcined at 1100˚C.

The temperature was raised from 900˚C to 1000˚C during non-fuel periods to investigate the release of oxygen for unsupported materials. By increasing temperature, the oxygen carriers are expected to release oxygen at higher oxygen partial pressure, see Figure 2. The results for the last periods with temperature increase are presented in Figure 5. As seen, the temperature increase leads to a significant oxygen release for materials with 20-40% manganese.

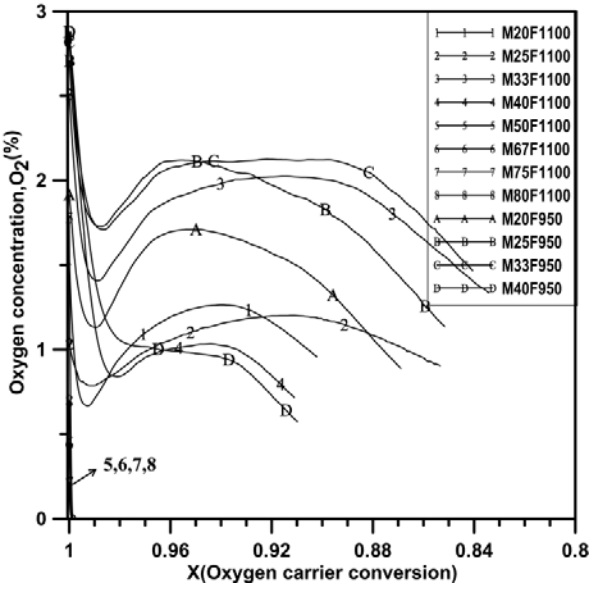

Figure 5- Oxygen concentration as a function of oxygen carrier conversion, X, during the last non-fuel period with temperature increase from 900˚C to 1000˚C for unsupported materials (paper II)

Figure 6 illustrates the concentration of O_2 as a function of Mn/(Mn+Fe) molar ratio at the end of the 300 s non-fuel periods for unsupported materials. From Figure 6 it can be concluded that the oxygen carriers with a Mn/(Mn+Fe) molar ratio in the range 20% to 40% release oxygen at 900˚C, whereas the materials with higher Mn-fraction show no oxygen release. Again, the explanation is that the oxygen carriers with a high Mn-fraction could not be oxidized to bixbyite at 900˚C at any feasible rate. Figure 6 shows that by decreasing the temperature from 900˚C to

850˚C, the oxygen release of material with a Mn/(Mn+Fe) molar ratio of 50% and higher is increased from 0% to 0.1-0.45%. Also, the particles with a calcination temperature of 950˚C show better oxygen release than the particles calcined at 1100˚C. Higher calcination temperature often gives lower porosity and lower reactivity.

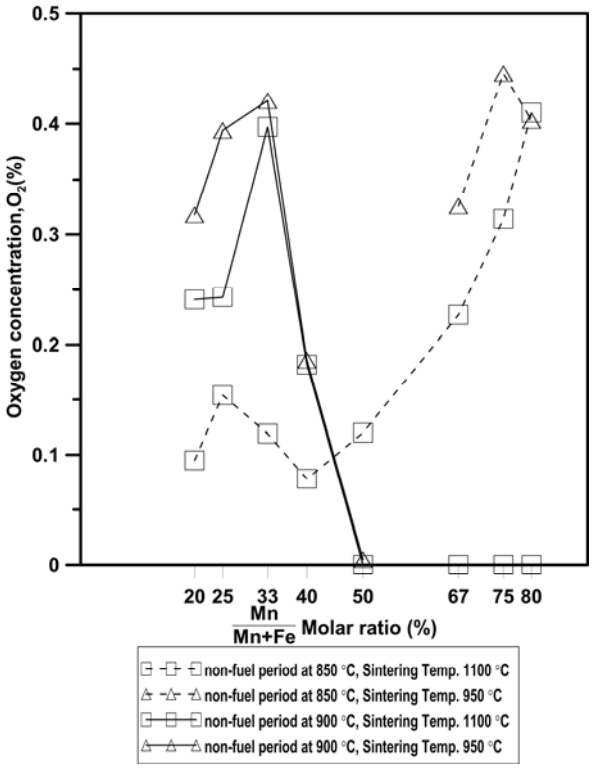

Figure 6- O_2 concentration as a function of Mn/(Mn+Fe) molar ratio at the end of the 300 s non-fuel periods at 900˚C and 850˚C for unsupported materials (paper II)

Support materials are often used together with active oxygen carriers in order to improve reactivity or mechanical properties. For instance, Al_2O_3, ZrO_2, TiO_2 or SiO_2 are examples of materials that have been used as support material[67]. Considering the promising results of the Mn Fe combined system as well as the problems with respect to mechanical stability, it is relevant to investigate the use of support materials for combined oxides of Fe-Mn.

In paper VI, addition of $MgAl_2O_4$, CeO_2, ZrO_2 and Y_2O_3-ZrO_2 as support to oxygen carriers with a Mn:Fe molar ratio of 75:25 has been investigated. Figure 7 illustrates the oxygen volume fraction as a function of time(s) during one inert period for the different oxygen carriers with a Mn:Fe molar ratio of 75:25 with addition of $MgAl_2O_4$, CeO_2, ZrO_2 and Y_2O_3-ZrO_2 as support.

Here the temperature is raised from 800˚C to 850˚C at the same time as the gas is switched from oxidizing to inert. The time needed for the temperature increase is around 250 s.

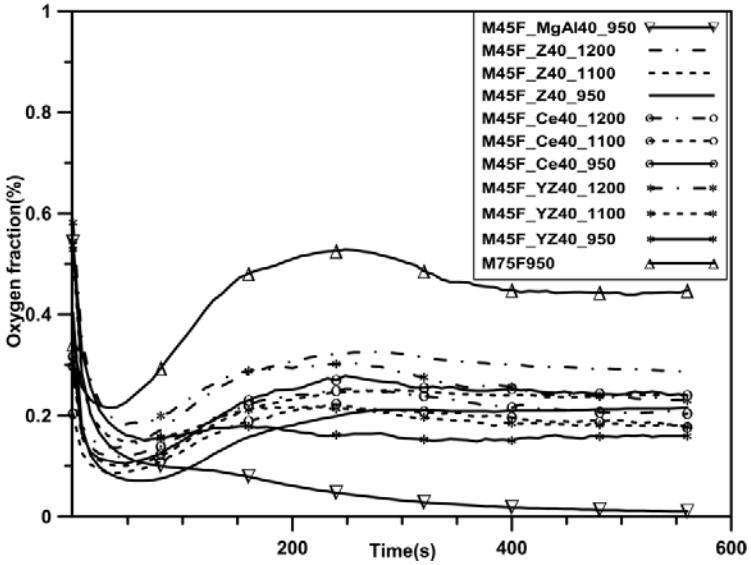

Figure 7- Oxygen volume fraction as a function of time(s) during the inert periods at 850˚C for oxygen carriers with a Mn:Fe molar ratio of 75:25 with addition of $MgAl_2O_4$, CeO_2, ZrO_2 and Y_2O_3-ZrO_2 as support (paper VI)

Figure 7 shows that the oxygen concentration for all materials except M45F_MgAl40_950 is in the range of around 0.2% to 0.5% during the inert period, with the highest release for the unsupported material. This may not be so surprising, considering that the amount of bed material is the same for all cases, meaning that the amount of active material is considerably less for the supported carriers. The measured oxygen volume fractions are much lower than those predicted by thermodynamics, which means that the oxygen concentrations measured are a result of kinetics. Still, there is a relatively large spread in the oxygen release rates for the different supports, with the best behaviour seen for the material produced with pure zirconia and calcined at 1200˚C, while the material with $MgAl_2O_4$ support had the least propensity to release oxygen. Hence, it seems as if the CLOU property, which is now well known for the pure combined oxide, is to a large extent retained using Ce and Zr-based supports.

Furthermore, a comprehensive study of the use of Al_2O_3 as oxygen carrier was made, see paper VII. Al_2O_3 has been found to be a suitable support for iron oxide[88-91], and thus it was decided to also pursue this system for the combined Mn-Fe system. Here, two sets of materials were produced using spray-drying: high-Fe materials with a Mn:Fe molar ratio of 33:67 and high-Mn

materials with a Mn:Fe molar ratio of 80:20. AlOOH was used for the preparation, which is transformed to Al_2O_3 during heat up. The Al content was varied for each set of materials.

Figure 8 shows the oxygen volume fraction as a function of time during one inert period for some materials with a Mn:Fe molar ratio of 80:20 with addition of Al_2O_3 as support. Here the temperature is raised from 800˚C to 850˚C at the same time as the gas is switched from oxidizing to inert. The O_2 concentration is in the range of around 0.2% to 0.5% with the highest release for the materials with lowest Al content calcined at 950˚C, M77FA3-950.

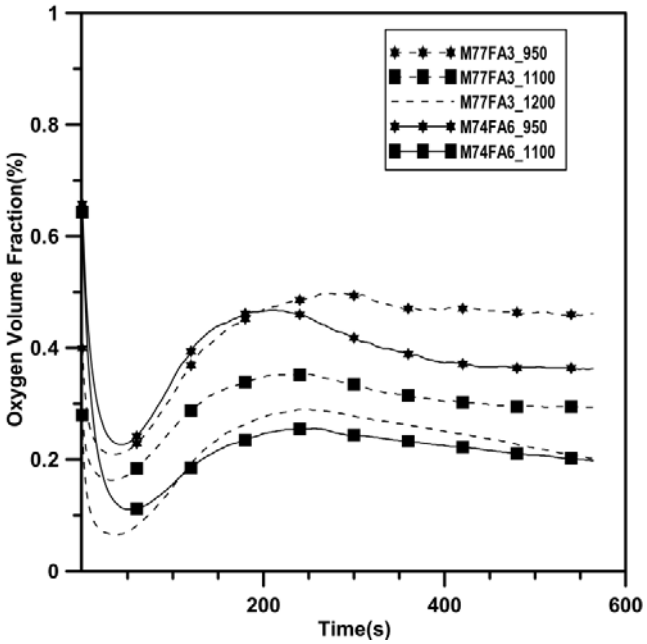

Figure 8- Oxygen volume fraction as a function of time(s) during the inert periods at 850˚C for materials with a Mn:Fe molar ratio of 80:20 and for materials with a Mn:Fe molar ratio of 80:20, all with addition of Al_2O_3 (paper VII)

Comparing Figure 7 and 8 indicates that materials with addition of Al_2O_3 showed higher oxygen release than the other support materials. Still, there were problems with oxidation for these materials at temperatures above 800˚C.

The oxygen carriers with higher iron content i.e. material with Mn/(Mn+Fe) molar ratio of 33%, showed high oxygen release, and the mechanical strength was higher compared with the material with high Mn-fraction. Also, the oxidation with 5 vol% of oxygen was possible at temperature higher than 850˚C. Figure 9 shows the volume fraction of O_2 at the end of the 300 s

inert period as a function of the AlOOH mass fraction added during production. As can be seen from Figure 9 the materials released more oxygen at higher temperature. The material with the lowest amount of Al had the highest rate of release. Generally, oxygen release falls with increasing Al content at lower reaction temperatures, but is more constant or even increases with Al content at high temperatures. At 1050˚C, M31FA3-1100 showed a very drastic decrease in oxygen release. Pressure drop measurements indicated defluidization at this temperature. Nonetheless, this material started to fluidize again as temperature was lowered and it was possible to run the final cycles at 900˚C. It should be noted that for M28FA14-1100, the measurements in the final cycle at 900˚C, was lost because of sampling error.

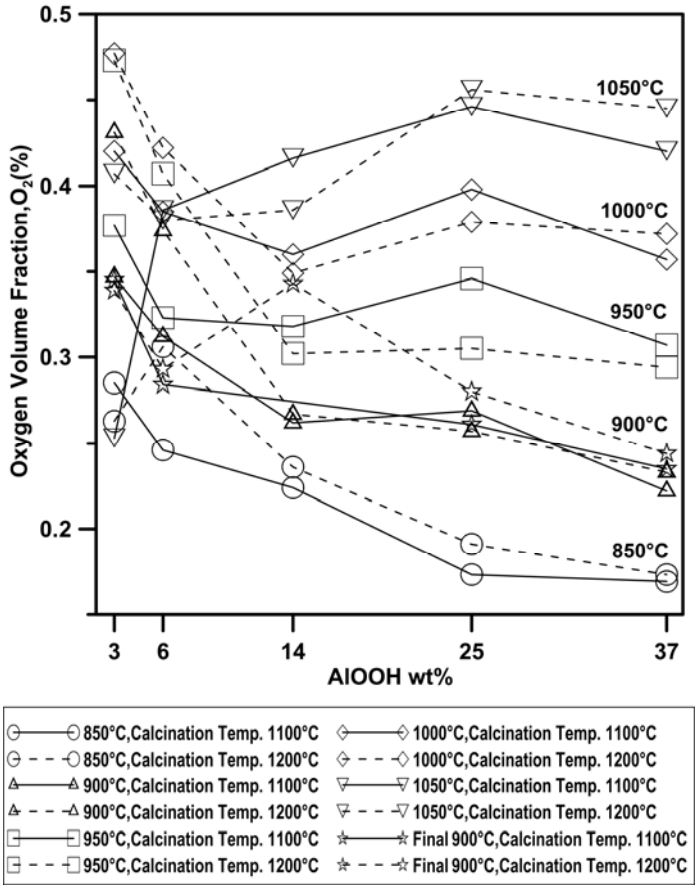

Figure 9- Volume fraction of O_2 at the end of the 300 s inert period at different temperatures as a function of AlOOH mass fraction, for materials with a Mn:Fe molar ratio of 33:67 (paper VII)

3.2.2 Conversion of the Oxygen Carriers with Gaseous Fuel

Figure 10 demonstrates the outlet dry gas concentration for reduction with CH_4 for a sample of unsupported material.

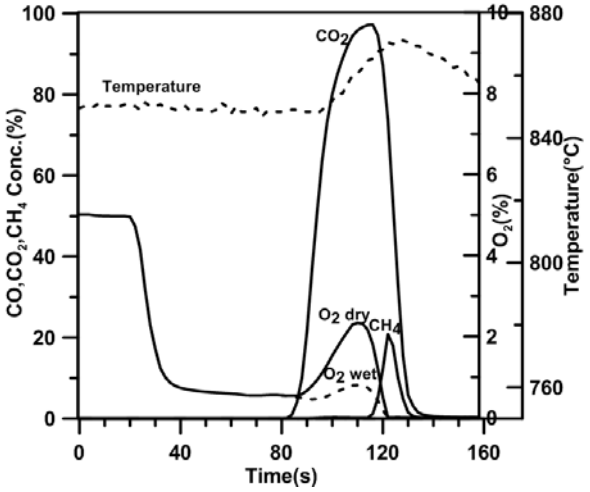

Figure 10- Measured dry gas concentrations during 40 s reduction of 15 g M80F950 with 365 mL_n/min CH_4 at 850 ˚C (paper IV)

In Figure 10 the air is shifted to nitrogen at the time 20 s. The figure shows that the iron manganese oxide spontaneously decomposes giving ≈0.6% of oxygen in the outlet gas. At the time 80 s gaseous fuel, methane, is added for 40 s. Methane reacts directly with the oxygen released from the $(Mn_{0.8},Fe_{0.2})_xO_y$ producing CO_2 and heat, which results in a temperature increase promoting the spontaneous release of O_2. The O_2 uncoupling was sufficiently fast for producing a concentration of CO_2 close to 100%. Before fuel is added the oxygen concentration is 0.5-0.6%, corresponding to an oxygen flow of 5 mL_n/min. The oxygen in the CO_2 comes from the oxygen carrier, so when fuel is added oxygen is released from the particles at a rate which is able to oxidize a methane flow of 365 mL_n/min, which means an oxygen flow of 730 mL_n/min from the particles. Thus, the oxygen release is increased by two orders of magnitude. At the same time the measured oxygen concentration, i.e. measured on dry basis, is increased by roughly a factor of three, see Figure 10. This is mainly an artifact caused by the steam produced in the reaction with methane, giving two H_2O per CO_2 in the outlet gas. Since the steam is removed before the analyzer the concentrations of the other gas components are overestimated. Figure 10 also shows the calculated O_2 concentration calculated on wet basis, i.e. the actual concentration at the outlet of the reactor, and as seen this is reasonably constant. This would also be expected if

the oxygen concentration is mainly controlled by the thermodynamic equilibrium. This suggests a very rapid O_2 release, considering the large quantities of oxygen consumed by the fuel. Another factor influencing the results is that the reaction between CH_4 and M80F950 is exothermic. Hence the temperature in the sample bed increases ≈20 K during experiments with CH_4, which should increase the equilibrium partial pressure of O_2 over the sample somewhat.

There is some backmixing of the gas before it reaches the analyzer. As seen in Figure 10, the initial transient in the O_2 concentration when nitrogen is turned on is approximately 10 s long. Similar transients of approximately 10 s due to back mixing are expected when oxygen release from the particles is slowing down and methane starts to appear in the outlet gas. This would explain the overlapping period in Figure 10 when O_2 and CH_4 are measured simultaneously during 10 s. The actual concentration of O_2 in the reactor likely goes to zero as methane starts to rise rapidly.

Figure 11a shows the gas conversion, γ, from equation 27, as a function of mass-based oxygen carrier conversion for unsupported materials at 950˚C with methane, cf. Table 1. The value for ω does not start at 1 because it decreases slightly due to release of oxygen during the short inert period before the reduction.

Figure 11a shows that the methane conversion for M25F950 and M33F950 are higher than for the others. The oxygen carriers with 50-80% manganese did not release any oxygen during non-fuel periods in inert atmosphere. The same particles showed some gas conversion during the reduction phase but it was generally lower compared to the other materials. All particles except, M67F1100, showed full conversion of syngas at 950˚C.

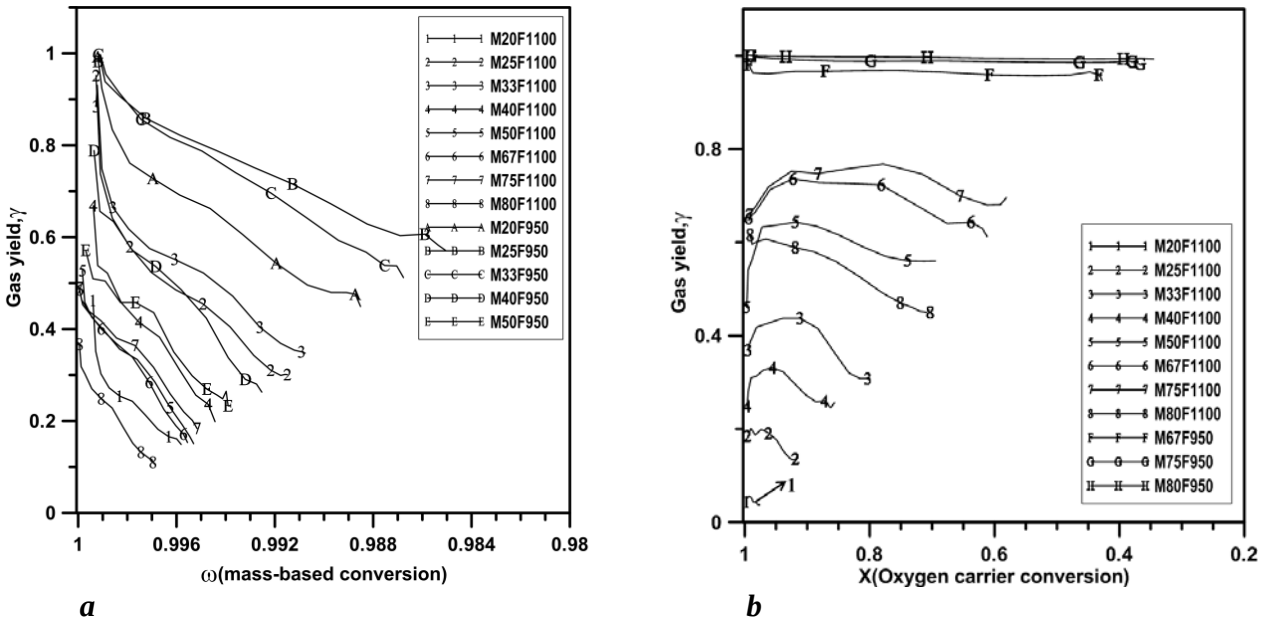

Figure 11- Gas conversion, γ , (a) vs. mass-based conversion, ω, at 950˚C and (b) vs. oxygen carrier conversion, X, at 850 ˚C using methane for 20 s for unsupported materials (paper II)

As stated before, the oxidation of the oxygen carriers with a Mn/(Mn+Fe) molar ratio higher than 50% would be difficult or impossible in the air reactor with 5% of oxygen at 900˚C or 950˚C. Therefore, at 950˚C, these particles are in the reduced spinel phase, $(Mn,Fe)_3O_4$, when introduced to the fuel reactor. Hence the methane conversion shown in Figure 11a is likely due to further reduction of $(Mn,Fe)_3O_4$ to MnO. The mass-based conversion, ω, is used in Figure 11a instead of X, because the X is defined based on the conversion of $(Mn,Fe)_2O_3$ to $(Mn,Fe)_3O_4$. For comparison to the other figures, the mass-based conversion, ω, can be converted to X using equation 26. Thus, a full conversion in the other figures corresponds to a change in ω of R_0=0.0336.

As discussed previously, applying a temperature lower than 900˚C in the air reactor should make it possible to oxidize the oxygen carriers with a Mn/(Mn+Fe) molar ratio higher than 50% to bixbyite. Hence, the materials were also tested at a lower temperature, i.e. 850˚C. In Figure 11b, gas conversion is plotted against oxygen carrier conversion using methane for 20 s at 850˚C.

As seen in Figure 11b, the reactivity of the oxygen carriers with a Mn/(Mn+Fe) molar ratio higher than 50%, increases when reducing the temperature to 850˚C whereas the reactivity decreases for materials with a Mn/(Mn+Fe) molar ratio of less than 50%. The particles with a

calcination temperature of 950˚C show better oxygen release and methane conversion than the particles calcined at 1100˚C. These observations were expected since the lower calcination temperature gives softer particles with more porosity which results in higher reactivity. The oxygen carriers M67F950, M75F950 and M80F950 have almost full conversion of methane to CO_2 and H_2O at 850˚C.

In Figure 12, the methane conversion, γ, is shown for an oxygen carrier conversion, ω, equal to 0.997, as a function of the Mn/(Mn+Fe) molar ratio for unsupported materials.

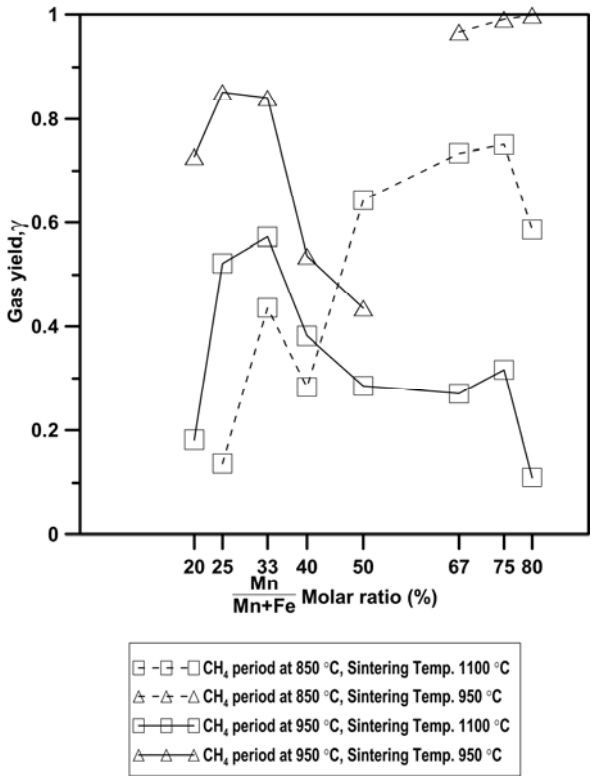

Figure 12- The methane conversion, γ, at 950˚C and 850˚C at ω = 0.997 versus Mn/(Mn+Fe) molar ratio for unsupported materials (paper II)

In Figure 12 the methane reactivity shows the same trend as the oxygen uncoupling properties in Figure 6. At the higher temperature, 950˚C, oxygen carriers with Mn/(Mn+Fe) molar ratio in the range of 25% to 33%, show the best gas conversion. At 850˚C, on the other hand, high methane conversion is seen for high Mn containing oxygen carriers.

Considering the fact that the Mn-Fe combined system shows very interesting properties with respect to reactivity, but because of problems with respect to mechanical stability, it is motivated to study the use of support materials.

Figure 13 shows the methane conversion, γ, as a function of mass-based oxygen-carrier conversion for oxygen carriers with a Mn:Fe molar ratio of 75:25 with addition of $MgAl_2O_4$, CeO_2, ZrO_2 and Y_2O_3-ZrO_2 as support. For comparison, also unsupported material with the same Mn/Fe ratio is included in the figure.

Figure 13 shows that the methane conversion for M75F950 and M45F_Z40_950 is higher than for the other investigated materials. Generally, all the particles except M45F_MgAl40_950 and M45F_Ce40_1200 have fairly high CH_4 conversion. The particles with a lower calcination temperature show better methane conversion than the particles calcined at higher temperature. Overall, the CH_4 conversion for the materials can be ranked according to the support used as follows: $ZrO_2 > Y_2O_3$-$ZrO_2 > CeO_2 > MgAl_2O_4$.

The unsupported M75F950 and the supported M45F_Z40_950 both convert methane to CO_2 and H_2O almost completely at 850˚C. These materials were able to transfer oxygen corresponding to almost 2.5% of their mass in 20 s. In Figure 13, only the unsupported M75F950 showed full gas yield throughout the whole period**,** but for M45F_Z40_950 the conversion almost remained at 1 and only at the end it decreases somewhat. However, this is not surprising since the amount of bed material is the same for all cases, meaning that the amount of active material is considerably less for the supported carriers.

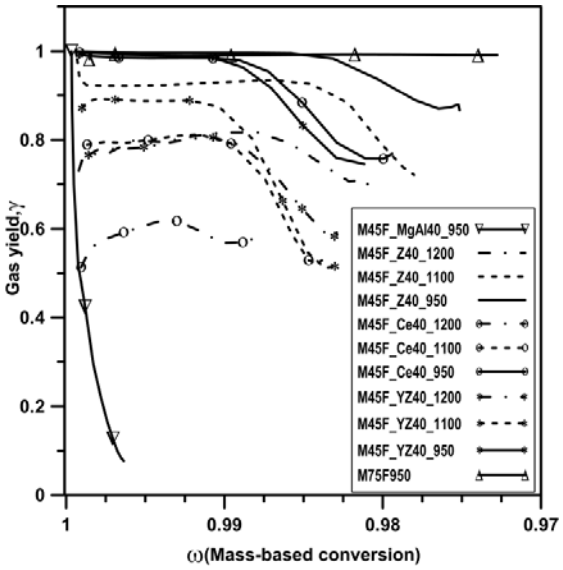

Figure 13- Gas yield, γ , vs. mass-based conversion, ω, using methane for 20 s at 850 ˚C for oxygen carriers with a Mn:Fe molar ratio of 75:25 with addition of $MgAl_2O_4$, CeO_2, ZrO_2 and Y_2O_3-ZrO_2 as support. The unsupported material M75F950 is included for comparison (paper VI)

From these experiments it is not possible to safely conclude which is the main mechanism for the oxygen transfer; whether the fuel reacts directly with the oxygen carrier or if the fuel reacts with the oxygen released. In previous work[94] with M75F950, solid fuel tests were performed which indicated that the main mechanism of the fuel conversion is via CLOU. Since M45F_Z40_950 shows similar behaviour as M75F950, it is likely that most or all of the oxygen is transferred via the CLOU mechanism, at least during the part of reaction period where there is full conversion of CH_4 and still a surplus of oxygen.

The oxygen carrier M45F_MgAl40_950 showed low release of oxygen and very low fuel conversion. This can be attributed to the fact that the particles could not be oxidized with 5% O_2 and therefore it was in its reduced form during the entire experiment. This material could not even be oxidized at 700˚C. This can be due to interaction of support with active materials. XRD results indicated that the $MgAl_2O_4$ is not an inert support and reacts with the iron manganese oxide.

In addition to the supports studied above, Al_2O_3 was also investigated, as discussed in the previous section. Figure 14 shows the methane conversion, γ, as a function of mass-based oxygen-carrier conversion for materials with a Mn:Fe molar ratio of 80:20 with addition of Al_2O_3 as support.

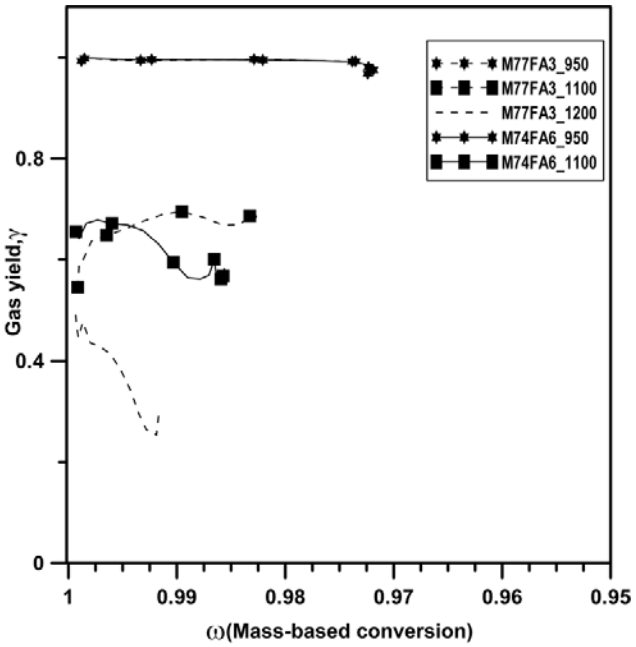

Figure 14- Gas yield, γ, vs. mass-based conversion, ω, using methane for 20 s at 850 ˚C for materials with a Mn:Fe molar ratio of 80:20 with addition of Al_2O_3 as support (paper VII)

Figure 14 shows that the methane conversion for M77FA3-950 and M74FA6-950 is higher than the other investigated materials with almost full conversion of methane to CO_2 and H_2O at 850˚C. Generally, the particles with a lower calcination temperature showed better methane conversion than the particles calcined at higher temperature. As mentioned in the previous section, it was not possible to oxidize materials with high Al-content.

The oxygen carriers with higher iron content i.e. material with Mn/(Mn+Fe) molar ratio of 33%, showed lower gas conversion, but the mechanical strength was higher compared with the material with high Mn-fraction. Also, the oxidation with 5 vol% of oxygen was possible at temperatures higher than 850˚C.

As said, addition of Al_2O_3 to materials with a Mn:Fe molar ratio of 33:67 was also investigated. In Figure 15 the methane conversion, γ , for mass-based oxygen-carrier conversion, ω, equal to 0.997, is shown as a function of the AlOOH mass fraction used during production. Clearly, the CH_4 conversion is higher at higher temperatures. The CH_4 conversion is highest for M20FA37-1100 and M24FA25-1100 at temperature above 950˚C.

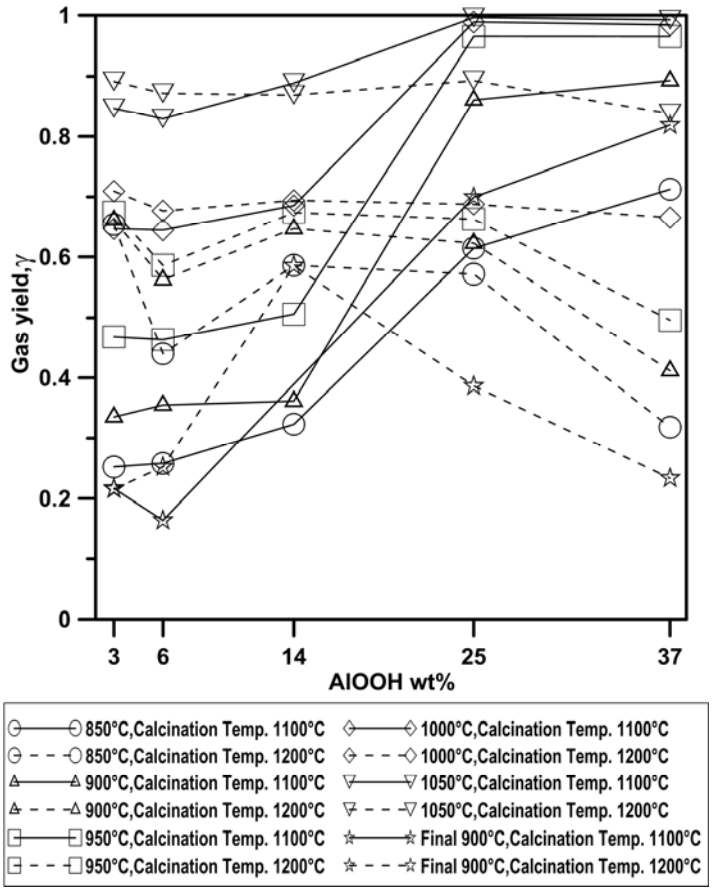

Figure 15- Gas yield, γ, at ω = 0.997 versus AlOOH mass fraction using methane for 20 s at different temperatures for materials with a Mn:Fe molar ratio of 33:67 with addition of Al_2O_3 as support calcined at 1100 and 1200˚C (paper VII)

Materials calcined at 1200˚C showed higher gas conversion with the exception of materials with ALOOH content of 25 wt% and higher. For these, the materials calcined at 1100˚C showed higher gas conversion. For materials calcined at 1100˚C, addition of more Al_2O_3 increases the CH_4 conversion. This may be associated with the higher BET surface area for these materials. But in the case of calcination at 1200˚C, addition of Al_2O_3 decreases the CH_4 conversion.

3.2.3 Oxygen carrier reactivity with solid fuels

In this work several experiments were made with Mn-Fe based oxygen carriers and solid fuels in order to better elucidate the CLOU reaction. In Figure 4a and 11a, the unsupported oxygen carrier M33F1100 shows good behaviour in terms of its oxygen release during non-fuel periods at 900˚C and methane conversion at 950˚C. Therefore, M33F1100 was also tested with a low-volatile solid fuel using inert fluidization gas, N_2. The char particles effectively remove the

released oxygen as they were converted to CO_2, hence increasing the driving force for oxygen release more effectively than when an inert gas such as nitrogen is introduced to the samples.

In figure 16 the corrected outlet gas concentrations, i.e. concentration before adding the sweep gas, are shown as a function of time for the reducing period and the following oxidation period for M33F1100 particles and petroleum coke at 950°C. The oxygen concentration at the end of the oxidation is 5% and when the fluidizing gas is switched to nitrogen it falls to around 1% which corresponds to the O_2 release by the carrier. When the fuel is introduced to the reactor a small peak of CH_4 and CO can be seen in the beginning of the reaction due to devolatilization of the fuel. Some volatiles react with the oxygen carrier and CO_2 increases rapidly. The oxygen concentration falls to zero as the fuel reacts rapidly with the oxygen released. When the devolatilization is finished, the remaining char can only be converted by reaction with oxygen released from the oxygen carrier. This is since the fluidizing gas is nitrogen, so there is no gasification of the char. Thus, the CO_2 is a measure of oxygen release. After switching to oxidizing gas, there is first a CO_2 peak, after which the oxygen increases. This is accompanied by a small increase in temperature as a result of the exothermic oxidation. The CO_2 peak shows that there is some fuel left in the bed which has not been converted.

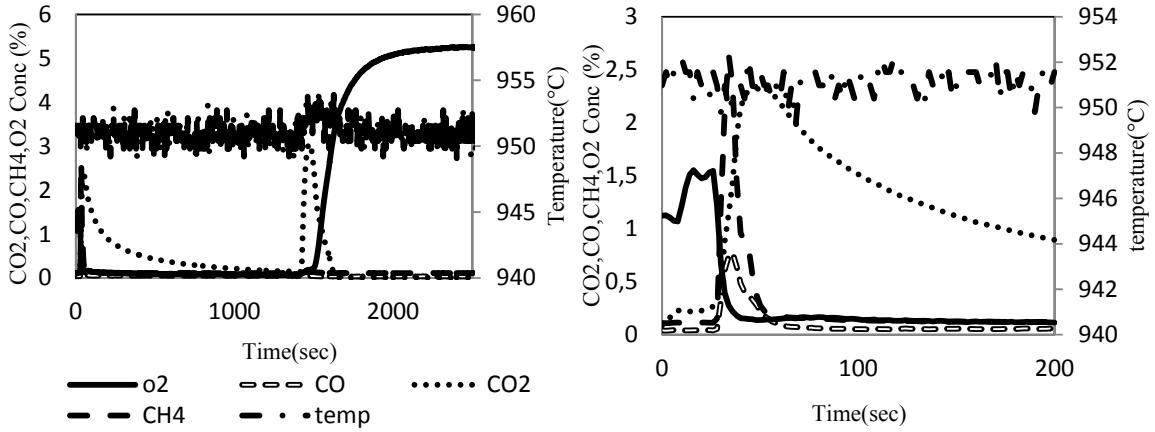

a ***b***

Figure 16- Concentrations for (a) the reduction and oxidation and (b) close-up of the reduction for a cycle with 0.1 g of petroleum coke in 20 g of M33F1100 particles at 950°C. The fluidizing gas in reduction is pure nitrogen (paper III)

Using petroleum coke as fuel at 900 and 1000°C shows a similar type of behaviour as the one shown in Figure 16, although the rate of reaction and the flue gas concentrations are different.

Figure 17 shows the corrected CO_2 concentration, i.e. the concentration before addition of sweep gas, as a function of mass-based conversion during reduction of 20 g M33F1100 with 0.1 g petroleum coke at 900, 950, 1000°C and also using steam at 950°C. The value for ω does not start at 1 because it decreases slightly due to release of oxygen during the short inert period before the reduction.

The change in mass-based conversion suggests that the oxygen-carrier particles are able to release oxygen corresponding to approximately 0.4% of their mass. The concentration of CO_2, which corresponds to the oxygen release rate when M33F1100 and fuel is fluidized by nitrogen, increases with temperature. Adding steam as fluidizing gas in the reduction period increases the CO_2 concentration as the char can also be gasified by steam. Thus, a combination of CLC and CLOU occurs, in other words both steam gasification, with syngas being oxidized by the oxygen carrier, and combustion of fuel through oxygen release by the particles. However, the increase in CO_2 and mass-based conversion resulting from the steam added is fairly moderate.

Moreover, for the test where steam was added in the fluidizing gas, the CO concentration falls to zero after devolatilization. This indicates full conversion of the gas, in contrast to experiments with oxygen carriers without release of gaseous oxygen, where there is a significant fraction of unconverted CO[95]. Thus, the tests indicate that this type of combined manganese-iron oxygen carrier, if used in chemical-looping of solid fuels, could contribute both to faster fuel conversion and to higher conversion of gas, as compared to oxygen-carrier materials that does not release oxygen. It should be noted that in all experiments, a CO_2 peak could be observed in the start of the oxidation period, which shows that the amount of fuel was in excess to remove oxygen released.

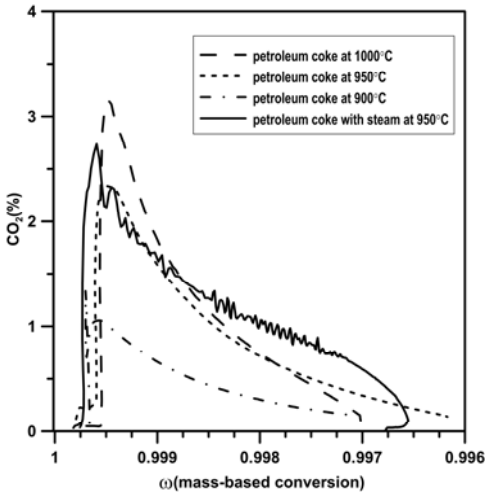

Figure 17- Corrected CO_2 concentration as a function of mass-based conversion, ω, during reduction of 20 g M33F1100 with 0.1 g petroleum coke (paper III)

In order to increase the mechanical stability of these combined materials, several supports have been employed, with varying degrees of success, see sections 3.2.1 and 3.2.2. One of the more interesting systems was the one including Al_2O_3, especially utilizing higher Fe-content, i.e. particles with a Mn:Fe molar ratio of 33:67. Some materials were investigated further with extra experiments with syngas and solid fuel as to obtain a better understanding of the behaviour of the samples with respect to reaction with solid fuels, i.e. coal or biofuels. The solid fuel experiments were designed as to get quantification of the release of oxygen. These results are presented in more detail in paper VII.

Figure 18a illustrates the oxygen carrier mass-based conversion, ω, vs. time during reduction with 0.2 g of devolatilized wood char at 950˚C. In these experiments, the char is fully devolatilized, therefore, the char can only be converted by reaction with oxygen released from the oxygen carrier. As the char is in excess and the fluidizing gas is nitrogen the emitted CO_2 is a measure of oxygen release.

Figure 18b shows mass-based conversion, ω, vs. time during reduction period of 3 g oxygen carrier with syngas at 950˚C. As shown in Figure 18a, M20FA37-1100 showed the fastest release of oxygen and it could release 2% of its mass in around 500 s. This should be compared to the syngas conversion where 1.8 wt% in around 10 s of oxygen reacted with syngas, see Figure 18b. Thus, it is quite clear that the oxygen release rate is much slower compared with the rate of oxygen carrier conversion in the presence of syngas. This indicates that the main mechanism of gas conversion is through the direct reaction for these materials.

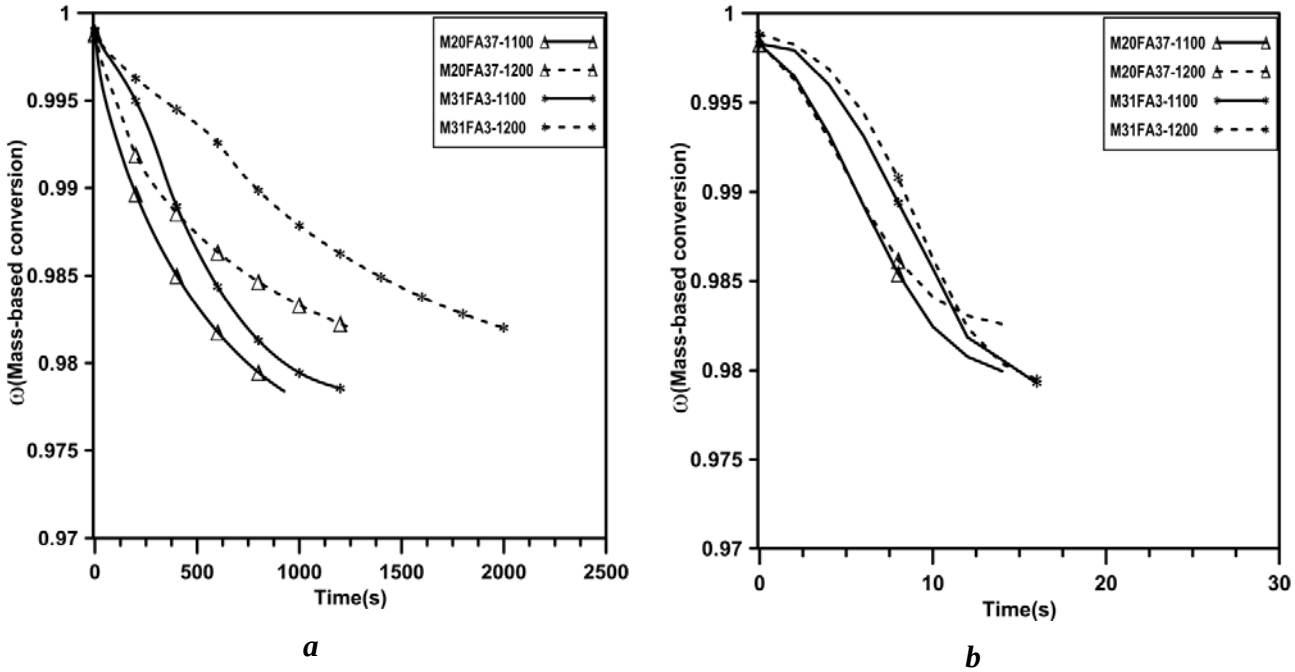

Figure 18- Oxygen carrier mass-based conversion, ω, as a function of time during reduction period of (a) 10 g oxygen carrier using 0.2 g of devolatilized wood char and (b) 3 g oxygen carrier with syngas at 950˚C (paper VII)

As seen in Figure 4b and 11b, the oxygen carriers M67F950, M75F950 and M80F950 show high oxygen release and almost full conversion of methane to CO_2 and H_2O at 850˚C. These are combined oxides with a higher fraction of Mn compared to Fe, and as explained earlier they have a higher propensity to release oxygen at lower temperatures compared to high-Fe materials. Tests were also performed with these materials using wood char in a similar way as above, with the aim of elucidating the dominating reaction pathway.

Data for one of the solid fuel tests with M80F950 is shown in Figure 19. Here, the corrected gas concentrations, i.e. gas concentrations corrected for dilution by the sweep gas, are shown as a function of time for reduction of 10 g M80F950 particles with 0.6 g wood char at 850˚C. The oxygen concentration during oxidation is 5%. When the fluidizing gas is switched to nitrogen, the oxygen concentration decreases to around ≈0.5%. When the fuel is introduced to the reactor, peaks of CH_4 and CO can be seen in the beginning of the reaction due to the presence of some volatile matter in the char. Simultaneously, the CO_2 concentration increases since the combustion of volatiles and char starts instantly. As the solid fuel enter the reactor, the oxygen concentration falls to zero as the fuel consumes all oxygen released. The absence of oxygen and the high

concentration of CO_2 show that the decomposition reaction of $(Mn,Fe)_2O_3$ to $(Mn,Fe)_3O_4$ is occurring without any thermodynamic barrier. When the rapid initial devolatilization is finished, the remaining char can only be converted by reaction with oxygen released from the oxygen carrier.

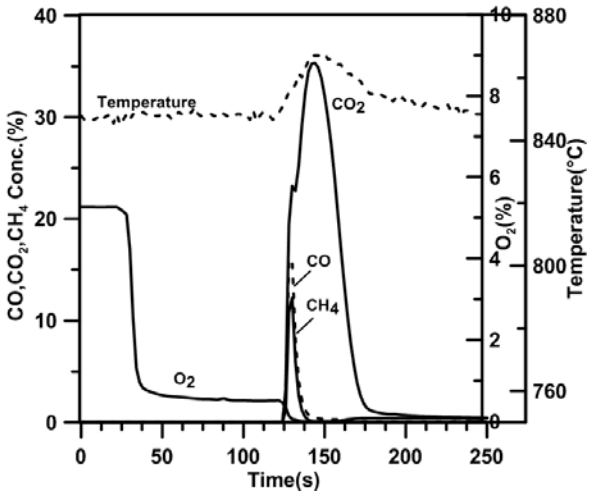

Figure 19- Measured dry gas concentrations during the reduction of 10 g M80F950 with 0.6 g wood char at 850˚C (paper IV)

The results from fuel tests using lower ratios of fuel to oxygen carrier particles showed similar behaviour, but with lower CO_2 concentration and higher O_2 levels, see paper IV. The oxygen concentration in these experiments does not fall to zero and also increases with increasing temperature due to the exothermic reaction of the fuel combustion. The excess of oxygen in these experiments shows that the amount of fuel for these cases was insufficient to remove all oxygen evolved, indicating that the fuel combustion, not the O_2 release, is limiting the overall reaction. In order to obtain a rate which is relevant for a well-functioning CLC system, the oxygen concentration in the bulk should approach zero. Figure 20 shows the oxygen carrier conversion as a function of time for both a CH_4 cycle and the solid fuel cycles. In Figure 20, time starts when fuel is added, and because of oxygen release during the preceding inert period, X is slightly less than 1. The denotation of $\frac{Fuel(g)}{O.C.(g)}$ in Figure 20, is used to indicate the ratio of the mass of wood char to oxygen carrier.

Figure 20 demonstrates that by increasing the mass ratio of fuel to oxygen carrier, the rate of oxygen carrier conversion also increases. It also shows that for full reduction of oxygen carrier (X=0), a sufficient amounts of fuel is needed. The test with the highest char to oxygen carrier

ratio, $\frac{Fuel(g)}{O.C.(g)} = \frac{0.6}{10}$, is the case where the maximum oxygen removal rate from the oxygen carrier was achieved. Here the oxygen carrier is almost fully reduced and the rate of oxygen carrier conversion is similar to the test with CH_4. This was also the only solid fuel test where the oxygen concentration reached zero.

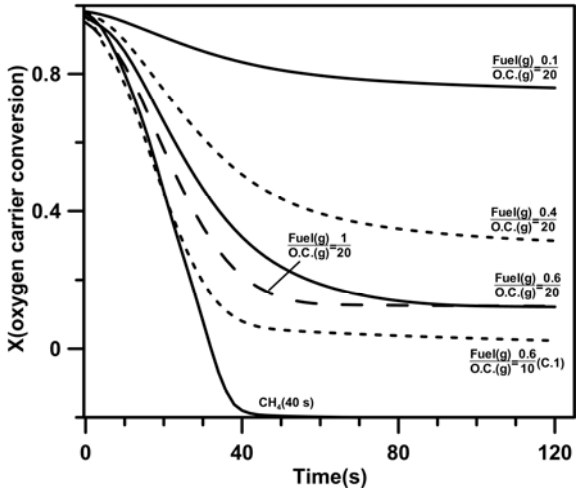

Figure 20- Oxygen carrier conversion,(X), vs. time for both CH_4 cycle and solid fuel cycles with M80F950 at 850˚C (paper IV)

Figure 20 shows that for the tests with $\frac{\boldsymbol{Fuel(g)}}{\boldsymbol{O.C.(g)}} = \frac{\boldsymbol{0.6}}{\boldsymbol{10}}$ and CH_4, the oxygen carrier becomes fully reduced in around 40 s. Considering concentration transients caused by the backmixing, the conversion time seen in Figure 20 is overestimated by around 10 s. Thus, most of the oxygen is released in about 30 s. Therefore, the particles were able to release oxygen corresponding to more than 3% of their mass in less than 40 s. The rapid release of oxygen in the solid fuel experiments, support the presumption that the main reaction mechanism between methane and M80F950 is by oxygen release in gas phase. This could be compared to the results of the Al_2O_3 supported material in Figure 18a, where considerably longer time is needed for the full release of oxygen, and this at a higher temperature. This illustrates that the identified optimum Mn-fraction of 60-80 mole% in the phase diagram in Figure 2, could be of very high interest, since both the thermodynamics and kinetics seem to support this. The problem seems to be associated with mechanical stability as well as the difficulties in oxidizing the materials at a sufficiently low partial pressure of oxygen, which will be discussed below.

3.2.4 Oxidation of the oxygen carrier particles

It is important that oxygen carriers can be oxidized at reasonable levels of oxygen in the gas phase. During experiments with M80F950, oxidation was slow and after more fuel cycles, the oxidation became slower. The difficulties with initiating the oxidation were solved by reducing the oxidation temperature to 800˚C. This is in accordance with thermodynamics, as a temperature decrease facilitates oxidation by lowering the equilibrium partial pressure. As mentioned previously, this is particular important for high-Mn oxygen carriers. In paper V, the oxygen carrier materials with Mn:Fe molar ratios in the range 67:33 up to 80:20 were examined with devolatilized wood char, in order to see how the iron content affects oxygen release and uptake. Thermodynamic analysis shows that increased iron content raises the temperature at which the material releases oxygen at a given partial pressure of oxygen. For a given temperature, increased iron content should therefore reduce the oxygen release but facilitate the oxygen uptake. Here oxygen release is investigated at 850˚C in cycles comprising oxidation by 5% oxygen in nitrogen followed by addition of devolatilized wood char in N_2.

The reduction with devolatilized wood char and the subsequent oxidation in 5% oxygen of M67F950, M75F950 and M80F950 were first investigated at 850˚C. The conversion was rapid during reaction with char, but difficulties with oxidation were seen already in the third cycle. In this respect there was no difference between the three materials investigated in this work, as problems with the oxidation of the materials started after approximately three cycles for all of them.

Further tests were therefore made with a lower oxidation temperature. In Figure 21, the corrected gas concentrations, i.e. gas concentrations corrected for dilution by the sweep gas, are shown as a function of time for (a) reduction of 10 g M80F950 with 0.3 g wood char at 850˚C and (b) the following oxidation period with 5% O_2 at 800˚C. Figure 21a shows the same trend as Figure 19 although the CO_2, CO and CH_4 peaks are lower because the wood char used here is devolatilized. Figure 21b shows the gas concentration during oxidation with 5% O_2. By switching the fluidizing gas to 5% O_2, the CO_2 concentration increases since the combustion of unconverted char starts. During this period all oxygen is consumed by the char, as the oxygen concentration is clearly too low to allow any oxidation of the oxygen carrier. As the char burns out the oxygen concentration starts to increase and stabilizes at the inlet concentration of approximately 5%. After some time the temperature of the oven is decreased to 800˚C, and the oxygen concentration

drops, indicating that the material is reacting with some of the supplied oxygen. The results for the other two investigated materials were similar to the results in Figure 21, except for small differences in concentrations.

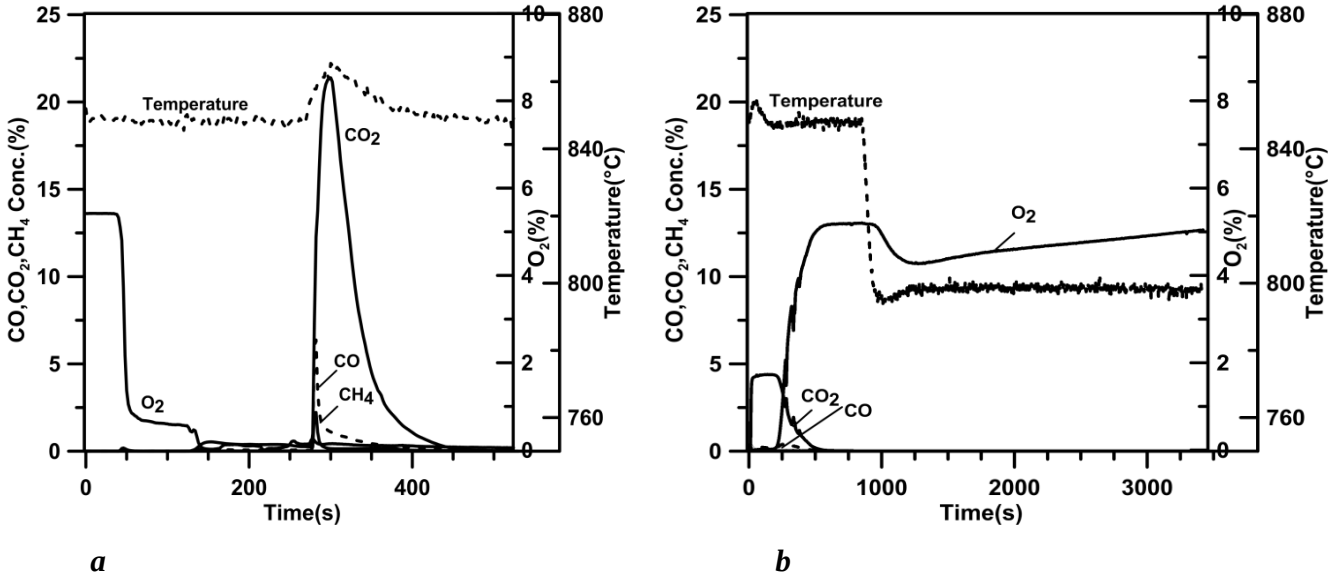

Figure 21- Measured dry gas concentrations during (a) the reduction of 10 g M80F950 with 0.3 g devolatilized wood char at 850˚C and (b) oxidation with 5% O_2 at 800˚C (paper V)

Figure 22 shows the oxygen carrier conversion as a function of time during (a) reduction of M67F950, M75F950 and M80F950 with devolatilized wood char at 850˚C and (b) oxidation with 5% O_2 at 800˚C.

In Figure 22a, time starts when fuel is added, and because of oxygen release during the preceding inert period, X is slightly less than 1. In all these tests the amount of inserted solid fuel was in excess whilst some CO_2 was observed during oxidation periods. All three materials show almost similar behaviour during the reduction period and released most of its oxygen in 80 s, as seen in Figure 22a. The rate of oxidation for all these three materials is slow, which can be attributed to the gas flow rate and the low oxygen content of this flow. Figure 22 shows that varying the iron content between 20% and 33% does not appear to have any strong effect on either oxygen release or oxygen uptake.

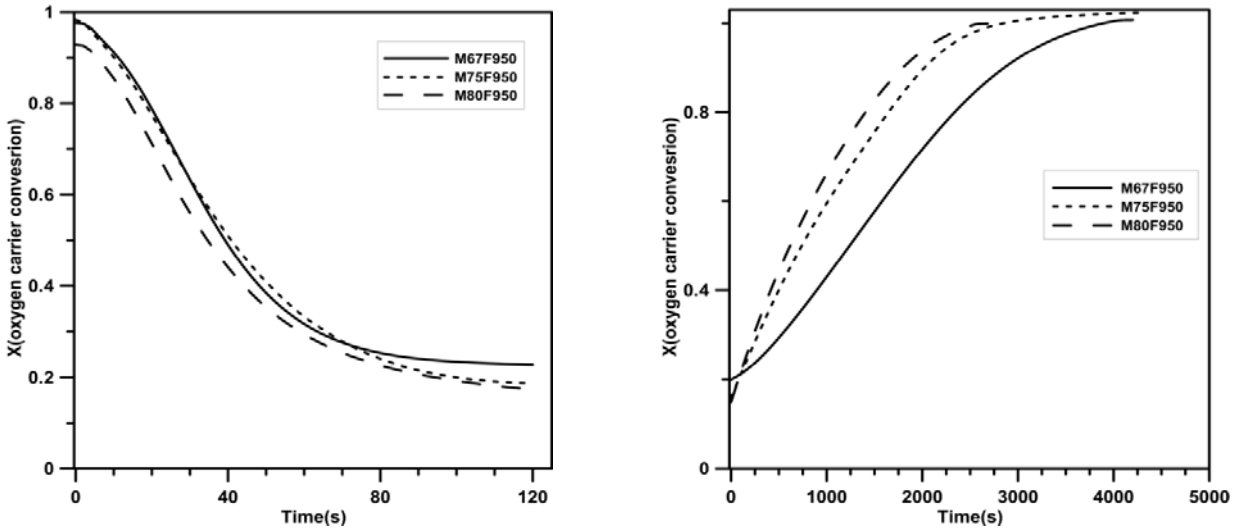

a *b*

Figure 22- Oxygen carrier conversion,(X), vs. time during (a) reduction period with wood char at 850˚C and (b) oxidation with 5% O_2 at 800˚C (paper V)

3.2.5 Analysis of the Oxygen Carrier Particles

3.2.5.1 Crystal structures (papers II,VI-VII)

The crystalline phase composition of the fresh unsupported Mn-Fe oxygen carriers was examined with X-ray powder diffraction. The identified phases were bixbyite and for high iron content material, hematite. However, there is a difficulty in safe analyses of this system as the XRD peaks of several of these compounds are close to each other, which is not surprising considering that the iron and manganese are neighbours in the periodic table. Some additional tests were performed with M33F950 particles in order to better elucidate the reduction mechanism. Here, a fresh sample was first reduced in 900˚C in N_2 until the measured oxygen concentration approached zero, at which point the sample was cooled in nitrogen and analysed with XRD. The same sample was then again heated in an inert atmosphere to 950˚C, and there exposed to methane during only a 10 s reduction. As can be seen in in Figure 23, the identified phases for fresh M33F950 are the bixbyite and hematite structure of $(Mn,Fe)_2O_3$ as expected. The sample reduced in nitrogen contained two phases: hematite $(Mn,Fe)_2O_3$ and the reduced spinel

phase $(Mn,Fe)_3O_4$. This is also expected from the phase relationships in Figure 2, since a complete reduction to spinel for material with this composition will occur only at a very high temperature or very low partial pressure of oxygen. Hence, as the partial pressure of oxygen is very low at 900˚C, complete reduction in nitrogen may take a long time, and thus the two identified species are expected. When this sample was heated to 950˚C, there was a release of oxygen, due to decomposition of the remaining hematite to spinel at the higher temperature. Further reduction with a 10 s pulse with CH_4 completely reduced the hematite to spinel, as can be seen in Figure 23.

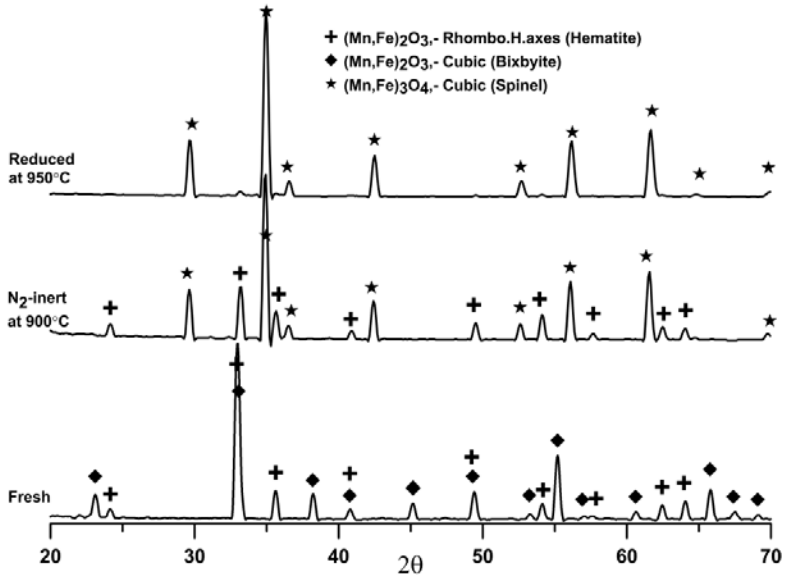

Figure 23- Diffractograms for fresh M33F950, reduced particles in N_2 at 900˚C and reduced particles with CH_4 at 950˚C (paper II)

The crystalline phase composition of the oxygen carriers with a Mn:Fe molar ratio of 75:25 with addition of $MgAl_2O_4$, CeO_2, ZrO_2 and Y_2O_3-ZrO_2 as support was examined with X-ray powder diffraction. The active phases identified of materials with CeO_2, ZrO_2 and Y_2O_3-ZrO_2 were similar to unsupported material, i.e. M75F950, again confirming the intact and operational combined oxide materials. The oxidized active phase in these samples is cubic bixbyite structure of $(Mn,Fe)_2O_3$ and the reduced phase is the tetragonal spinel structure of $(Mn,Fe)_3O_4$. The additional inert phase in the material with ZrO_2 as support is the monoclinic structure of ZrO_2 both in the reduced and oxidized states. For ZrO_2-supported material sintered at 1200˚C, some tetragonal or cubic structure of ZrO_2 was also seen. With Y_2O_3-ZrO_2 as support, the cubic or

tetragonal structure of Y_2O_3-ZrO_2 was identified, and with CeO_2 as support, the cubic structure of CeO_2 was seen. In the case of CeO_2, some small fraction of Fe or Mn could possibly be mixed with CeO_2.

The phase identified for the material with $MgAl_2O_4$ as support, M45F_MgAl40_950, was $Mg_xFe_yMn_zAl_{3-x-y-z}O_4$. This indicates that the $MgAl_2O_4$ is not an inert support and reacts with the iron manganese oxide. Judging from the reactivity experiments, this phase is apparently rather inactive for reactions with methane and syngas.

The phase analysis support the reactivity results that CeO_2, ZrO_2 and Y_2O_3-ZrO_2 could be possible candidates as support for the oxygen-carrier materials based on Mn-Fe whereas the $MgAl_2O_4$ is a poor candidate. However, based on the attrition data, only the ZrO_2 showed substantial improvement compared to the unsupported oxygen carrier.

The crystalline phase composition of the oxygen carriers with a Mn:Fe molar ratio of 33:67 with addition of Al_2O_3 as support was examined with X-ray powder diffraction. The oxidized phases are $(Fe,Al)_2O_3$, corundum, or $(Mn,Fe)_2O_3$, bixbyite, and the reduced phase is $(Mn,Fe,Al)_3O_4$-spinel. It should be noted that the XRD-patterns of $(Mn,Fe,Al)_3O_4$ and $(Mn,Fe)_3O_4$ are similar, and therefore it was hard to differentiate between these. The fresh materials contained both reduced and oxidized phases. In general, by increasing Al content, more Al was seen in this structure. Therefore, with lower Al, mostly $(Mn,Fe)_3O_4$ could be expected. The $(Mn,Fe)_2O_3$ was mostly seen for materials with lower Al content. By increasing Al content more $(Fe,Al)_2O_3$ was seen.

3.2.5.2 Crushing strength (papers II-VII)

The crushing strength of unsupported Mn-Fe oxygen carriers varies between 0.1 – 1.7 N and is generally higher for higher Fe content. There was less of an effect of the calcination temperature, although for high-Fe materials the crushing strength is somewhat higher for materials treated at 1100˚C. Although the relation between crushing strength and attrition is not clear, it can be expected that material with too low crushing strength will break in a real unit. For comparison, the crushing strength of a Ni-based oxygen carrier successfully operated in continuous fluidized bed CLC reactor for 1000 h was 2.3 N[96].

The crushing strength of the oxygen carriers with a Mn:Fe molar ratio of 75:25 with addition of $MgAl_2O_4$, CeO_2, ZrO_2 and Y_2O_3-ZrO_2 varies between 0.4 – 1 N. Generally the crushing strength increases as a function of calcination temperature. However, for the materials with ZrO_2

the crushing strength is somewhat lower for materials sintered at higher temperature. This can be attributed to crystal structure transformation of ZrO_2 at higher temperature. ZrO_2 has monoclinic crystal structure at temperatures below 1170˚C and with increasing temperature it changes to tetragonal and cubic structure which has smaller volume[97]. Therefore, cooling of these materials results cracks due to induced stresses as a result of volume expansion of crystal structure transformation from the cubic to tetragonal to monoclinic[97].

This explanation correlates well with the XRD analysis of these materials which showed that the inert phase in the material with ZrO_2 as support is the monoclinic structure of ZrO_2 both in the reduced and oxidized states. For ZrO_2-supported material sintered at 1200˚C, some tetragonal or cubic structure of ZrO_2 was also seen. Thus, the calcination temperature could be of substantial importance, and it is advised not to use too high calcination temperatures for ZrO_2-supported material.

The crushing strength of the oxygen carriers with a Mn:Fe molar ratio of 33:67 with addition of Al_2O_3 as support varies between 0.6 – 1.7 N with the highest crushing strength for materials with lowest addition of Al, M31FA3. Generally the crushing strength and density increase as a function of calcination temperature.

3.2.5.3 Attrition resistance (papers VI-VII)

Attrition tests were performed using a customized jet cup rig, which was briefly described above The following particles were tested: oxygen carriers with a Mn:Fe molar ratio of 75:25 with addition of $MgAl_2O_4$, CeO_2, ZrO_2 and Y_2O_3-ZrO_2 as support and also materials with a Mn:Fe molar ratio of 33:67 and 80:20 supported with Al_2O_3. As a reference, the attrition index of an unsupported material with a Mn:Fe molar ratio of 33:67, which is M33F1100 and also unsupported material with a Mn:Fe molar ratio of 75:25 were also measured. Among materials with a Mn:Fe molar ratio of 75:25, all the materials except M45F_Z40_950 showed very poor attrition resistance and were fragmented or turned to dust. For M45F_Z40_950 an attrition index, Ai of 8.5 wt%/h was found, and also had the highest crushing strength in this group of materials.

Attrition tests were performed on the fresh materials with a Mn:Fe molar ratio of 80:20 supported with Al_2O_3 i.e. M77FA3 calcined at 950, 1100 and 1200˚C, M74FA6 calcined at 950, 1100 and 1200˚C, M50FA37 calcined at 950 and 1200˚C. All the materials except those calcined at 1200˚C showed very poor attrition resistance and were fragmented or turned to dust. For materials calcined at 1200˚C, an attrition index, Ai of 1.2-1.8 wt%/h was found.

The results for materials with a Mn:Fe molar ratio of 33:67 supported with Al_2O_3 indicated good attrition resistance for all materials except M24FA25-1100, with attrition indices, Ai of 0.45-3.7 wt%/h. For comparison, the attrition behaviour of unsupported material, M33F1100, was poor with Ai of 30 wt%/h.

4 Discussion

In the last five years, there has been a significant number of investigations of materials for CLOU, with a focus on Cu-based materials. As Cu-materials may have drawbacks with respect to cost, agglomeration and stability, it is motivated to also investigate other materials which have the ability to release gas phase oxygen at relevant conditions. There are several combined oxide systems which may be of interest, whereof the Mn-Fe combination is one of the more promising[98]. This work is the first comprehensive investigation of the Fe-Mn-O system for Chemical-Looping with Oxygen Uncoupling (CLOU), where materials with varying Mn/Fe ratios have been investigated with respect to oxygen release and reactivity with gaseous and solid fuels. The results clearly illustrate that this system could have great promise, as many of the materials release a fair amount of oxygen at relevant conditions. This uncoupling effect gives an important advantage when used with solid fuels, as the gasification reactions needed with normal CLC are fully or partially avoided, thus promoting char conversion. But CLOU materials will also have advantages over non-CLOU materials in converting gaseous fuels. Due to the low price and favourable environmental properties of manganese and iron oxides, these findings could be of great importance for the development of chemical-looping combustion with oxygen uncoupling. The materials used in this work are manufactured which is associated with a production cost. A cheaper alternative for these materials would be natural ores, or waste products from industry. It is well known that naturally occurring manganese ores often contain high fraction of iron, in addition to other impurities, such as Si, Ca and Al. The price of manganese ore (metallurgical grade) has varied between 100 and 800 $/ton in the last ten years[99], with the most current prices around 200–300 $/ton.

In a CLC system, it is important to keep the air ratio low in order to improve efficiency, which means that the oxygen concentration from the air reactor should be as low as possible. In this work, 5% O_2 was employed, which corresponds to an air ratio of about 1.2 in an actual CLC system. The results presented above showed that the reduced form of the oxygen carriers with a Mn/(Mn+Fe) molar ratio of more than 50% would be difficult or impossible to oxidize to $(Mn,Fe)_2O_3$ at 950˚C and 900˚C because they are in or very close to the phase regions of bixbyite + spinel or spinel at a partial pressure of O_2 of 0.05 atm. Therefore, applying a lower temperature of 850˚C will improve the reoxidation of these oxygen carriers. It should be mentioned that this thermodynamic restriction only applies to the air reactor, and the temperature of the fuel reactor

could be higher, which would likely enhance the overall kinetics and the equilibrium oxygen partial pressure. A higher temperature in the fuel reactor is possible since the overall reactions in the fuel reactor for a high Mn-fraction oxygen carrier are exothermic.

The rate of oxygen release is directly proportional to the solids inventory of oxygen carrier in the fuel reactor. To illustrate the implications of the rates measured for M80F950 at 850˚C, an example is given here. If it is assumed that the oxygen carrier transfers oxygen corresponding to 2% of its mass in each cycle, this would correspond to a solids circulation between air and fuel reactor of 230 kg/min,MW using wood char as fuel. The presented rates of oxygen release suggest that a residence time of less than 30 s could be sufficient for the release of oxygen in presence of fuel. This would then, with the given circulation rate correspond to a solids inventory of only 115 kg/MW for the fuel reactor.

Although some of the unsupported materials worked excellently in laboratory, their mechanical strength and attrition resistance needed improvement in order to have sufficient durability for commercial application. Therefore, a series of supported materials with a Mn:Fe molar ratio of 80:20 with addition of $MgAl_2O_4$, CeO_2, ZrO_2, Y_2O_3-ZrO_2 and Al_2O_3 were investigated with the aim of increasing the attrition resistance. Based on the results from the reactivity tests and the measured attrition rates for all the particles, ZrO_2 support seems to be the most promising candidate among different supports for materials with high Mn-content. Unfortunately, addition of support to these materials had the drawback that these could not be oxidized at 850˚C and a decrease in temperature to 800˚C was needed in order to be able to oxidize the materials back to their fully oxidized state.

For materials with higher iron content, the oxidation with 5 vol% of oxygen was possible at temperatures higher than 850˚C, which is also in agreement with the phase compositions predicted by thermodynamics. Therefore, addition of Al_2O_3 to materials with a Mn:Fe molar ratio of 33:67 was investigated. Almost all Al_2O_3 supported high Fe-materials had good attrition resistance compared with unsupported materials as well as the other supported materials. Among the Al_2O_3 supported materials with a Mn:Fe molar ratio of 33:67, M20FA37-1100 showed the fastest release of oxygen and it could release 2% of its mass in around 500 s with solid fuel. The comparison between gaseous and char conversion shows that the conversion with gaseous fuels is reached within a much shorter period of time, in order of tens of seconds. The char conversion in N_2 is controlled by the oxygen release. As the oxygen release rate is much smaller compared to

the overall rate of oxygen carrier conversion in syngas or CH_4 conversion, the main mechanism of conversion of gaseous fuel is through the direct reaction. But the problem associated with mechanical stability as well as the difficulties in oxidizing the materials have been solved, and it is likely that also a partial, but slower, uncoupling effect could have significant advantages in a real system with respect to fuel conversion.

5 Conclusions

The influence of the steam and hydrogen concentration on the rate of char conversion in CLC was investigated. The oxygen exchange model was found to be the best in describing hydrogen inhibition mechanism in steam gasification. Thus, a strong dependency between fuel gasification rate and hydrogen concentration was found, indicating that it is desirable to use a reactive oxygen carrier which removes hydrogen efficiently.

Oxygen carrier materials of the combined oxide system Fe-Mn-O have been investigated with respect to chemical-looping combustion and chemical-looping with oxygen uncoupling. At the higher reaction temperature, 950˚C, oxygen carriers with a Mn/(Mn+Fe) molar ratio in the range of 25-33%, show the highest oxygen uncoupling properties and best methane conversion. At 850˚C, on the other hand, high methane conversion and oxygen release are seen for particles with a high Mn/(Mn+Fe) molar ratio, 67-80%. In fact the oxygen carriers with the latter ratio calcined at 950˚C gave almost full conversion of methane to CO_2 and H_2O at 850˚C. The rapid release of oxygen was also verified using wood char as fuel, where any solid-solid reaction between char and oxide particles would be negligible. It is shown that these materials are able to release gas phase oxygen corresponding to up to around 3.4% of its mass. Moreover, most of this oxygen can be released in only 30-40 s in presence of a fuel that maintains an oxygen partial pressure close to zero.

Addition of support to materials with a high Mn-fraction had the drawback that they could not be oxidized at 850˚C and to be able to oxidize them it was necessary to decrease the temperature to 800˚C. Based on the results from the reactivity tests and the measured attrition rates for all the particles, ZrO_2 support seems to be the most promising candidate among different supports for materials with a high Mn-fraction.

Most Al_2O_3-supported materials with a Mn:Fe molar ratio of 33:67 had good attrition resistance, with an attrition index, in range 0.45 to 3.7 wt%/h. In comparison, the attrition behaviour of the corresponding unsupported material, M33F1100, was poor with an attrition index of 30 wt%/h. Furthermore, some of these materials showed good reactivity with methane and syngas. Experiments with char showed that these materials were able to release large quantities of oxygen, i.e. up to 2% of the mass. This means that they are suitable for CLOU. However, the release is slow and it is clear that the main reaction mechanism with gaseous fuels

is not through oxygen release. Low attrition, good reactivity and CLOU properties in combination with potentially low raw materials costs, make these materials interesting for CLC.

6 References

1. Stocker, T. F., D. Qin, G.-K. Plattner, M. Tignor, S. K. Allen, J. Boschung, A. Nauels, Y. Xia, V. Bex and P.M. Midgley (eds.) *Summary for Policymakers*; In: Climate Change 2013: The Physical Science Basis. Contribution of Working Group I to the Fifth Assessment Report of the Intergovernmental Panel on Climate Change. Cambridge University Press, Cambridge, United Kingdom and New York, NY, USA., 2013.
2. Intergovernmental Panel on Climate Change(IPCC), Climate change 2001: the scientific basis, Cambridge: Cambridge University Press.
3. Davison, J., Performance and costs of power plants with capture and storage of CO_2. *Energy* **2007,** 32, (7), 1163-1176.
4. Zanganeh, K. E.; Shafeen, A., A novel process integration, optimization and design approach for large-scale implementation of oxy-fired coal power plants with CO2 capture. *International Journal of Greenhouse Gas Control* **2007,** 1, (1), 47-54.
5. Thiruvenkatachari, R.; Su, S.; An, H.; Xiang Yu, X., Post combustion CO_2 capture by carbon fibre monolithic adsorbents. *Progress in Energy and Combustion Science* **2009,** 35, (5), 438-455.
6. Kovscek, A. R.; Cakici, M. D., Geologic storage of carbon dioxide and enhanced oil recovery. II. Cooptimization of storage and recovery. *Energy Conversion and Management* **2005,** 46, (11-12), 1941-1956.
7. Freund, P.; Ormerod, W. G., Progress toward storage of carbon dioxide. *Energy Conversion and Management* **1997,** 38, Supplement, (0), S199-S204.
8. Manancourt, A.; Gale, J., A review of capacity estimates for the geological storage of carbon dioxide. *Greenhouse Gas Control Technologies 7* **2005**, 2051-2054.
9. Cooper, C., A technical basis for carbon dioxide storage. *Energy Procedia* **2009,** 1, (1), 1727-1733.
10. Anon, L., Testing CO2 —enhanced coalbed methane recovery. *Greenhouse Issues* **1999,** 9, (45), 1-3.
11. B. Toftegaard, M.; Brix, J.; A. Jensen, P.; Glarborg, P.; D. Jensen, A., Oxy-fuel combustion of solid fuels. *Progress in Energy and Combustion Science* **2010,** 36, (5), 581–625.
12. Buhre, B. J. P.; Elliott, L. K.; Sheng, C. D.; Gupta, R. P.; Wall, T. F., Oxy-fuel combustion technology for coal-fired power generation. *Progress in Energy and Combustion Science* **2005,** 31, (4), 283-307.
13. Lee, H. J.; Lee, J. D.; Linga, P.; Englezos, P.; Kim, Y. S.; Lee, M. S.; Kim, Y. D., Gas hydrate formation process for pre-combustion capture of carbon dioxide. *Energy* **2010,** 35, (6), 2729-2733.
14. Lyngfelt, A.; Leckner, B.; Mattisson, T., A fluidized-bed combustion process with inherent CO_2 separation; application of chemical-looping combustion. *Chemical Engineering Science* **2001,** 56, (10), 3101-3113.
15. Lewis, W. K.; Gilliland, E. R. Production of pure carbon dioxide. 1954.
16. Ishida, M.; Jin, H., A new advanced power-generation system using chemical-looping combustion. *Energy (Oxford, United Kingdom)* **1994,** 19, (4), 415-422.
17. Lyngfelt, A., Chemical looping combustion. In *Fluidized-bed technologies for near-zero emission combustion and gasification*, Scala F., Woodhead Publishing Limited: 2013; pp 895-930 (DOI: 10.1533/9780857098801.4.895).
18. Lyngfelt, A., Chemical-looping combustion of solid fuels – Status of development. *Applied Energy* **2014,** 113, (0), 1869-1873.
19. Lyngfelt, A., Oxygen Carriers for Chemical-Looping Combustion, submitted for inclusion as Chapter 11, in "Calcium and chemical looping technology for power generation and carbon dioxide (CO_2) capture" Eds Fennell, P., and Anthony, E.J.".
20. Fan, L. S.; Zeng, L.; Wang, W.; Luo, S., Chemical looping processes for CO_2 capture and carbonaceous fuel conversion - Prospect and opportunity. *Energy and Environmental Science* **2012,** 5, (6), 7254-7280.
21. Fang, H.; Haibin, L.; Zengli, Z., Advancements in Development of Chemical-Looping Combustion: A Review. *International Journal of Chemical Engineering,doi:10.1155/2009/710515* **2009**.
22. Hossain, M.; De Lasa, H., Chemical looping combustion (CLC) for inherent CO2 separations-a review. *Chemical Engineering Science* **2008,** 63, 4433-4451.
23. Adanez, J.; Abad, A.; Garcia-Labiano, F.; Gayan, P.; Diego, L. F., Progress in Chemical-Looping Combustion and Reforming technologies. *Progress in Energy and Combustion Science* **2012,** 38, 215-282.
24. Lyngfelt, A.; Thunman, H., Construction and 100 h of operational experience of a 10-kW chemical-looping combustor. *Carbon Dioxide Capture for Storage in Deep Geologic Formations--Results from the CO_2 Capture Project* **2005,** 1, 625-645.
25. Ryu, H.-J.; Jin, G.-T.; Bae, D.-H.; Yi, C.-K., Continuous Operation of a 50kWth Chemical-Looping Combustor: Long-Term Operation with Ni- and Co-Based Oxygen Carrier Particles. *Presented at the 5th China-*

Korea Joint Workshop on Clean Energy Technology, October 25-28, Qingdao University, China, 2004 **2004**, 221-230.
26. Abad, A.; Mattisson, T.; Lyngfelt, A.; Ryden, M., Chemical-looping combustion in a 300 W continuously operating reactor system using a manganese-based oxygen carrier. *Fuel* **2006,** 85, (9), 1174-1185.
27. Adanez, J.; Gayan, P.; Celaya, J.; de Diego, L. F.; Garcia-Labiano, F.; Abad, A., Chemical Looping Combustion in a 10 kWth Prototype Using a CuO/Al_2O_3 Oxygen Carrier: Effect of Operating Conditions on Methane Combustion. *Industrial & Engineering Chemistry Research* **2006,** 45, 6075-6080.
28. Johansson, E.; Mattisson, T.; Lyngfelt, A.; Thunman, H., A 300 W laboratory reactor system for chemical-looping combustion with particle circulation. *Fuel* **2006,** 85, (10-11), 1428-1438.
29. de Diego, L. F.; Garcia-Labiano, F.; Gayan, P.; Celaya, J.; Palacios, J. M.; Adanez, J., Operation of a 10 kWth chemical-looping combustor during 200 h with a $CuO-Al_2O_3$ oxygen carrier. *Fuel* **2007,** 86, 1036-1045.
30. Linderholm, C.; Abad, A.; Mattisson, T.; Lyngfelt, A., 160 hours of chemical-looping combustion in a 10 kW reactor system with a NiO-based oxygen carrier. *International Journal of Greenhouse Gas Control* **2008,** 2, (4), 520-530.
31. Leion, H.; Mattisson, T.; Lyngfelt, A., The use of petroleum coke as fuel in chemical-looping combustion. *Fuel* **2007,** 86, (12-13), 1947-1958.
32. Scott, S. A.; Dennis, J. S.; Hayhurst, A. N.; Brown, T., In situ gasification of a solid fuel and CO_2 separation using chemical looping. *AIChE Journal* **2006,** 52, (9), 3325-3328.
33. Brown, T. A.; Dennis, J. S.; Scott, S. A.; Davidson, J. F.; Hayhurst, A. N., Gasification and Chemical-Looping Combustion of a Lignite Char in a Fluidized Bed of Iron Oxide. *Energy Fuels* **2010,** 24, 3034-3048.
34. Mattisson, T.; Leion, H.; Lyngfelt, A., Chemical-looping with oxygen uncoupling using CuO/ZrO_2 with petroleum coke. *Fuel* **2009,** 88, (4), 683-690.
35. Eyring, E.; Konya, G.; Lighty, J.; Sahir, A.; Sarofim , A.; Whitty, K., Chemical Looping with Copper Oxide as Carrier and Coal as Fuel. *Oil & Gas Science and Technology* **2011,** 66, 209-221.
36. Berguerand, N.; Lyngfelt, A., Design and Operation of a 10 kWth Chemical-Looping Combustor for Solid Fuels – Testing with South African Coal. *Fuel* **2008,** 87, (12), 2713-2726.
37. Shen, L.; Wu, J.; Gao, Z.; Xiao, J., Reactivity deterioration of NiO/Al_2O_3 oxygen carrier for chemical looping combustion of coal in a 10 kWth reactor. *Combustion and Flame* **2009,** 156, (7), 1377-1385.
38. Cuadrat, A.; Abad, A.; García-Labiano , F.; Gayán, P.; de Diego, L. F.; Adánez, J., The use of ilmenite as oxygen-carrier in a 500 Wth Chemical-Looping Coal Combustion unit. *International Journal of Greenhouse Gas Control* **2011,** 5, (6), 1630–1642.
39. Adánez-Rubio, I.; Gayán, P.; Abad, A.; García-Labiano, F.; de Diego, L. F.; Adánez, J., CO_2 capture in coal combustion by chemical-looping with oxygen uncoupling (CLOU) with a Cu-based oxygen-carrier. *In: Proc. 5th Int Conf on Clean Coal Technologies (CCT2011). Zaragoza, Spain* **2011**.
40. Linderholm, C.; Schmitz, M.; Knutsson, P.; Källén, M.; Lyngfelt, A., Use of Low-Volatile Solid Fuels in a 100 kW Chemical-Looping Combustor. *Energy & Fuels* **2014,** 28, (9), 5942-5952.
41. Markström, P.; Linderholm, C.; Lyngfelt, A., Chemical-looping combustion of solid fuels – Design and operation of a 100kW unit with bituminous coal. *International Journal of Greenhouse Gas Control* **2013,** 15, (0), 150-162.
42. Leion, H.; Mattisson, T.; Lyngfelt, A., Solid Fuels in Chemical-Looping Combustion. *International Journal of Greenhouse Gas Control* **2008,** 2, 180-193.
43. Arjmand, M.; Leion, H.; Lyngfelt, A.; Mattisson, T., Use of Manganese Ore in Chemical-Looping Combustion (CLC)- Effect on Steam Gasification. *International Journal of Greenhouse Gas Control* **2012,** 8, 56-60.
44. Wen, Y.-y.; Li, Z.-s.; Xu, L.; Cai, N.-s., Experimental Study of Natural Cu Ore Particles as Oxygen Carriers in Chemical Looping with Oxygen Uncoupling (CLOU). *Energy Fuels* **2012,** 26, (6), 3919–3927.
45. Boot-Handford, M. E.; Abanades, J. C.; Anthony, E. J.; Blunt, M. J.; Brandani, S.; Mac Dowell, N.; Fernández, J. R.; Ferrari, M. C.; Gross, R.; Hallett, J. P.; Haszeldine, R. S.; Heptonstall, P.; Lyngfelt, A.; Makuch, Z.; Mangano, E.; Porter, R. T. J.; Pourkashanian, M.; Rochelle, G. T.; Shah, N.; Yao, J. G.; Fennell, P. S., Carbon capture and storage update. *Energy and Environmental Science* **2014,** 7, (1), 130-189.
46. Ströhle, J.; Orth, M.; Epple, B., Design and operation of a 1MWth chemical looping plant. *Applied Energy* **2014,** 113, 1490-1495.
47. Shen, L.; Wu, J.; Gao, Z.; Xiao, J., Reactivity deterioration of NiO/Al2O3 oxygen carrier for chemical looping combustion of coal in a 10 kWth reactor. *Combustion and Flame* **2009,** 156, (7), 1377-1385.
48. Bayham, S. C.; Kim, H. R.; Wang, D.; Tong, A.; Zeng, L.; McGiveron, O.; Kathe, M. V.; Chung, E.; Wang, W.; Wang, A.; Majumder, A.; Fan, L. S., Iron-based coal direct chemical looping combustion process: 200-h continuous operation of a 25-kWth subpilot unit. *Energy and Fuels* **2013,** 27, (3), 1347-1356.

49. Thon, A.; Kramp, M.; Hartge, E. U.; Heinrich, S.; Werther, J., Operational experience with a system of coupled fluidized beds for chemical looping combustion of solid fuels using ilmenite as oxygen carrier. *Applied Energy* **2014,** 118, 309-317.
50. Markström, P.; Linderholm, C.; Lyngfelt, A., Chemical-looping combustion of solid fuels – Design and operation of a 100 kW unit with bituminous coal. *International Journal of Greenhouse Gas Control* **2013,** 15, (0), 150-162.
51. Song, T.; Wu, J.; Zhang, H.; Shen, L., Characterization of an Australia hematite oxygen carrier in chemical looping combustion with coal. *International Journal of Greenhouse Gas Control* **2012,** 11, 326-336.
52. Gayán, P.; Forero, C. R.; Abad, A.; De Diego, L. F.; García-Labiano, F.; Adánez, J., Effect of support on the behavior of Cu-based oxygen carriers during long-term CLC operation at temperatures above 1073 K. *Energy and Fuels* **2011,** 25, (3), 1316-1326.
53. Pröll, T.; Kolbitsch, P.; Bolhàr-Nordenkampf, J.; Hofbauer, H., Chemical looping pilot plant results using a nickel-based oxygen carrier. *Oil & Gas Science and Technology* **2011,** 66, (2), 173-180.
54. Lyngfelt, A.; Kronberger, B.; Adanez, J.; Morin, J.-X.; Hurst, P., Development of oxygen carrier particles for chemical-looping combustion. Design and operation of a 10 kW chemical-looping combustor. *Greenhouse Gas Control Technologies* **2005,** 7, 115-123(7th International Conference on Greenhouse Gas Control Technologies, Vancouver, Canada, 5th-9th September 2004).
55. Moldenhauer, P.; Rydén, M.; Mattisson, T.; Lyngfelt, A., Chemical-looping combustion and chemical-looping with oxygen uncoupling of kerosene with Mn- and Cu-based oxygen carriers in a circulating fluidized-bed 300 W laboratory reactor. *Fuel Processing Technology* **2012,** 104, (0), 378-389.
56. Leion, H., Lyngfelt, A. and Mattisson, T., Effects of steam and CO2 in the fluidizing gas when using bituminous coal in chemical-looping combustion. *Proceedings of The 20th International Conference on Fluidized Bed Combustion, Xian, China* **2009**, (1), 608-611.
57. Dennis, J. S.; Scott, S. A.; Hayhurst, A. N., In situ gasification of coal using steam with chemical looping: a technique for isolating CO2 from burning a solid fuel. *Journal of the Energy Institute* **2006,** 79, (3), 187-190.
58. Hüttinger, K. J.; Merdes, W. F., The carbon-steam reaction at elevated pressure: Formations of product gases and hydrogen inhibitions. *Carbon* **1992,** 30, (6), 883-894.
59. Weeda, M.; Abcouwer, H.; Kapteijn, F.; Moulijn, J., Steam gasification kinetics and burn-off behavioiur for a bituminous coal derived char in the presence of H2. *Fuel Processing Technology* **1993,** 36, 235-242.
60. Lussier, M. G.; Zhang, Z.; J. Miller, D., Characterizing rate inhibition in steam/hydrogen gasification via analysis of adsorbed hydrogen. *Carbon* **1998,** 36, (9), 1361-1369.
61. Zhang, L.; Huang, J.; Fang, Y.; Wang, Y., Gasification Reactivity and Kinetics of Typical Chinese Anthracite Chars with Steam and CO2. *Energy Fuels* **2006,** 20, (3), 1201-1210.
62. Everson, R. C.; Neomagus , H.; Kasaini, H.; Njapha, D., Reaction kinetics of pulverized coal-chars derived from inertinite-rich coal discards: Gasification with carbon dioxide and steam. *Fuel* **2006,** 85, 1076–1082.
63. Keller, M.; Leion, H.; Mattisson, T.; Lyngfelt, A., Gasification inhibition in Chemical Looping Combustion with solid fuels. *Combustion and Flame* **2011,** 158, (3), 393-400.
64. Mattisson, T.; Lyngfelt, A.; Leion, H., Chemical-looping with oxygen uncoupling for combustion of solid fuels. *International Journal of Greenhouse Gas Control* **2009,** 3, (1), 11-19.
65. Leion, H.; Mattisson, T.; Lyngfelt, A., Using chemical-looping with oxygen uncoupling (CLOU) for combustion of six different solid fuels. *Energy Procedia* **2009,** 1, (1), 447-453.
66. Mattisson, T.; Lyngfelt, A.; Cho, P., The use of iron oxide as an oxygen carrier in chemical-looping combustion of methane with inherent separation of CO2. *Fuel* **2001,** 80, (13), 1953-1962.
67. Abad, A.; Mattisson, T.; Lyngfelt, A.; Johansson, M., The Use of Iron Oxide as Oxygen Carrier in a Chemical-Looping Reactor. *Fuel* **2007,** 86, 1021-1035.
68. Lyngfelt, A., Oxygen Carriers for Chemical Looping Combustion-4000 h of Operational Experience. *Oil & Gas Science and Technology - Revue D Ifp Energies Nouvelles* **2011,** 66, (2), 161-172.
69. Lyngfelt, A.; Mattisson, T., Materials for chemical-looping combustion. *In Efficient Carbon Capture for Coal Power Plants, Editors D. Stolten and V. Sherer, WILEY-VCH Verlag GmbH & Co. KGaA, Weinheim* **2011**.
70. Adánez-Rubio, I.; Abad, A.; Gayán, P.; de Diego, L. F.; García-Labiano, F.; Adánez, J., Identification of operational regions in the Chemical-Looping with Oxygen Uncoupling (CLOU) process with a Cu-based oxygen carrier. *Fuel* **2012,** 102, (0), 634-645.
71. Chuang, S. Y.; Dennis, J. S.; Hayhurst, A. N.; Scott, S. A., Development and performance of Cu-based oxygen carriers for chemical-looping combustion. *Combustion and Flame* **2008,** 154, (1–2), 109-121.

72. Zafar, Q.; Abad, A.; Mattisson, T.; Gevert, B.; Strand, M., Reduction and oxidation kinetics of Mn_3O_4/Mg–ZrO_2 oxygen carrier particles for chemical-looping combustion. *Chemical Engineering Science* **2007,** 62, 6556 – 6567.
73. Shulman, A.; Cleverstam, E.; Mattisson, T.; Lyngfelt, A., Manganese/Iron, Manganese/Nickel, and Manganese/Silicon Oxides Used in Chemical-Looping With Oxygen Uncoupling (CLOU) for Combustion of Methane. *Energy Fuels* **2009,** 23, 5269-5275.
74. Shulman, A.; Cleverstam, E.; Mattisson, T.; Lyngfelt, A., Chemical – Looping with oxygen uncoupling using Mn/Mg-based oxygen carriers – Oxygen release and reactivity with methane. *Fuel* **2011,** 90, (3), 941-950.
75. Leion, A.; Larring, Y.; Bakken, E.; Bredesen, R., Use of $CaMn_{0.875}Ti_{0.125}O_3$ as Oxygen Carrier in Chemical-Looping with Oxygen Uncoupling. *Energy & Fuels* **2009,** 23, 5276-5283.
76. Bakken, E.; Norby, T.; Stølen, S., Nonstoichiometry and reductive decomposition of $CaMnO_{3-\delta}$. *Solid State Ionics* **2005,** 176, (1-2), 217-223.
77. Rydén, M.; Lyngfelt, A.; Mattisson, T., $CaMn_{0.875}Ti_{0.125}O_3$ as oxygen carrier for chemical-looping combustion with oxygen uncoupling (CLOU)–experiments in a continuously operating fluidized bed reactor system. *International Journal of Greenhouse gas control* **2011,** 5, 356-366.
78. Crum, J. V.; Riley, B. J.; Vienna, J. D., Binary Phase Diagram of the Manganese Oxide – Iron Oxide System. *J. Am. Ceram. Soc* **2009,** 92, 2378-2384.
79. Wickham, D., The chemical composition of spinels in the system Fe_3O_4-Mn_3O_4. *Journal of Inorganic and Nuclear Chemistry* **1969,** 31, 313-320.
80. Pishahang, M.; Larring, Y.; McCann, M.; Bredesen, R., $Ca_{0.9}Mn_{0.5}Ti_{0.5}O_{3-\delta}$: A suitable oxygen carrier material for fixed-bed chemical looping combustion under syngas conditions. *Industrial and Engineering Chemistry Research* **2014,** 53, (26), 10549-10556.
81. Pishahang, M.; Bakken, E.; Stølen, S.; Thomas, C. I.; Dahl, P. I., Oxygen non-stoichiometry, redox thermodynamics, and structure of $LaFe_{1-x}Co_xO_{3-\delta}$. *Ionics* **2013,** 19, (6), 869-878.
82. Ksepko, E.; Siriwardane, R.; Tian, H.; Simonyi, T.; Poston, J.; Sciazko, M., Effect of H_2S on Chemical-Looping Combustion of Coal-Derived Synthesis Gas over Fe_2O_3 – MnO_2 Supported on ZrO_2/Sepiolite. In *1st International Conference on Chemical Looping, Lyon*, 2010.
83. Lambert, A.; Delquié, C.; Clémeneçon, I.; Comtea, E.; Lefebvrea, V.; Rousseau, J.; Durand, B., Synthesis and characterization of bimetallic Fe/Mn oxides for chemical looping combustion. *Energy Procedia* **2009,** 1, (1), 375-381.
84. Fossdal, A.; Bakken, E.; Øye, B. A.; Schøning, C.; Kaus, I.; Mokkelbost, T.; Larring, Y., Study of inexpensive oxygen carriers for chemical looping combustion. *International Journal of Greenhouse Gas Control* **2011,** 5, (3), 483-488.
85. Rydén, M.; Lyngfelt, A.; Mattisson, T., Combined manganese/iron oxides as oxygen carrier for chemical looping combustion with oxygen uncoupling (CLOU) in a circulating fluidized bed reactor system. *Energy Procedia* **2011,** 4, (0), 341-348.
86. Kjellqvist, L.; Selleby, M., Thermodynamic Assessment of the Fe-Mn-O System. *Journal of Phase Equilibria and Diffusion* **2010,** 31, (2), 113-134.
87. Muan, A.; Sōmiya, S., The system of iron oxide-manganese oxide in air. *American Journal of Science* **1962,** 260, 230-240.
88. He, F.; Wang, H.; Dai, Y., Application of Fe_2O_3/Al_2O_3 Composite Particles as Oxygen Carrier of Chemical Looping Combustion. *Journal of Natural Gas Chemistry* **2007,** 16, (2), 155-161.
89. Wang, B.; Yan, R.; Lee, D. H.; Zheng, Y.; Zhao, H.; Zheng, C., Characterization and evaluation of Fe_2O_3/Al_2O_3 oxygen carrier prepared by sol–gel combustion synthesis. *Journal of Analytical and Applied Pyrolysis* **2011,** 91, (1), 105-113.
90. Chiu, P.-C.; Ku, Y.; Wu, Y.-L.; Wu, H.-C.; Kuo, Y.-L.; Tseng, Y.-H., Characterization and Evaluation of Prepared Fe_2O_3/Al_2O_3 Oxygen Carriers for Chemical Looping Process. *Aerosol and Air Quality Research* **2014,** 14, (3), 981-990.
91. Ishida, M.; Takeshita, K.; Suzuki, K.; Ohba, T., Application of Fe_2O_3−Al_2O_3 Composite Particles as Solid Looping Material of the Chemical-Loop Combustor. *Energy & Fuels* **2005,** 19, (6), 2514-2518.
92. Rydén, M.; Moldenhauer, P.; Lindqvist, S.; Mattisson, T.; Lyngfelt, A., Measuring attrition resistance of oxygen carrier particles for chemical looping combustion with a customized jet cup. *Powder Technology* **2014,** DOI: 10.1016/j.powtec.2014.01.085.
93. Leion, H.; Jerndal, E.; Steenari, B.-M.; Hermansson, S.; Israelsson, M.; Jansson, E.; Johnsson, M.; Thunberg, R.; Vadenbo, A.; Mattisson, T.; Lyngfelt, A., Solid fuels in chemical-looping combustion using oxide scale and unprocessed iron ore as oxygen carriers. *Fuel* **2009,** 88, (10), 1945-1954.

94. Azimi, G.; Leion, H.; Rydén, M.; Mattisson, T.; Lyngfelt, A., Solid fuel conversion of iron manganese oxide as oxygen carrier for chemical-looping with oxygen uncoupling (CLOU). In *2nd International Conference on Chemical Looping*, Darmstadt, 26-28 September 2012.
95. Leion, H.; Jerndal, E.; Steenari, B.; Hermansson, S.; Mikael Israelssona, E. J., Martin Johnssona, Rebecka Thunberga, Albin Vadenboa, Tobias Mattissonb, Anders Lyngfeltb, Solid fuels in chemical-looping combustion using oxide scale and unprocessed iron ore as oxygen carriers. *Fuel* **2009,** 88, (10), 1945-1954.
96. Linderholm, C.; Mattisson, T.; Lyngfelt, A., Long-term integrity testing of spray-dried particles in a 10 kW chemical-looping combustor using natural gas as fuel. *Fuel* **2009,** 88, 2083-2096.
97. Chevalier, J.; Gremillard, L.; Virkar, A. V.; Clarke, D. R., The tetragonal-monoclinic transformation in zirconia: Lessons learned and future trends. *Journal of the American Ceramic Society* **2009,** 92, (9), 1901-1920.
98. Rydén, M.; Leion, H.; Mattisson, T.; Lyngfelt, A., Combined oxides as oxygen carrier material for chemical-looping with oxygen uncoupling. In *2nd International Conference on Chemical Looping*, Darmstadt, 26-28 September 2012.
99. U.S. Geological Survey, 2011. Mineral Commodity Summaries. ISBN 978-1-4113-3083-2.